

1 Seawater pH reconstruction using boron isotopes in multiple planktonic foraminifera species with  
2 different depth habitats and their potential to constrain pH and pCO<sub>2</sub> gradients  
3  
4

5 Maxence Guillermic<sup>1,2</sup>, Sambuddha Misra<sup>3,4</sup>, Robert Eagle<sup>1,2</sup>, Alexandra Villa<sup>2,5</sup>, Fengming Chang<sup>6</sup>,  
6 Aradhna Tripathi<sup>1,2</sup>  
7  
8  
9  
10

11 <sup>1</sup> Department of Earth, Planetary, and Space Sciences, Department of Atmospheric and Oceanic  
12 Sciences, Institute of the Environment and Sustainability, UCLA, University of California – Los  
13 Angeles, Los Angeles, CA 90095 USA

14 <sup>2</sup> Laboratoire Géosciences Océan UMR6538, UBO, Institut Universitaire Européen de la Mer, Rue  
15 Dumont d'Urville, 29280, Plouzané, France

16 <sup>3</sup> Indian Institute of Science, Centre for Earth Sciences, Bengaluru, Karnataka 560012, India

17 <sup>4</sup> The Godwin Laboratory for Palaeoclimate Research, Department of Earth Sciences, University of  
18 Cambridge, UK

19 <sup>5</sup> Department of Geology, University of Wisconsin-Madison, Madison, WI 53706 USA

20 <sup>6</sup> Key Laboratory of Marine Geology and Environment, Institute of Oceanology, Chinese Academy of  
21 Sciences, Qingdao 266071, China  
22  
23  
24  
25  
26  
27  
28  
29  
30  
31  
32  
33  
34  
35  
36

37 Submitted to Biogeosciences  
38  
39  
40

41 \*Corresponding authors:

42 E-mail address: maxence.guillermic@gmail.com, atripati@ucla.edu  
43

44 **ABSTRACT**

45

46 Boron isotope systematics of planktonic foraminifera from core-top sediments and culture experiments have been  
47 studied to investigate the sensitivity of  $\delta^{11}\text{B}$  of calcite tests to seawater pH. However, our knowledge of the  
48 relationship between  $\delta^{11}\text{B}$  and pH remains incomplete for many taxa. Thus, to expand the potential scope of  
49 application of this proxy, we report  $\delta^{11}\text{B}$  data for 7 different species of planktonic foraminifera from sediment  
50 core-tops. We utilize a method for the measurement of small samples of foraminifera and calculate the  $\delta^{11}\text{B}$ -calcite  
51 sensitivity to pH for *Globigerinoides ruber*, *Trilobus sacculifer* (sacc or w/o sacc), *Orbulina universa*, *Pulleniatina*  
52 *obliquiloculata*, *Neogloboquadrina dutertrei*, *Globorotalia menardii* and *Globorotalia tumida*, including for  
53 unstudied core-tops and species. These taxa have diverse ecological preferences and are from sites that span a  
54 range of oceanographic regimes, including some that are in regions of air-sea equilibrium and others that are out  
55 of equilibrium with the atmosphere. The sensitivity of  $\delta^{11}\text{B}_{\text{carbonate}}$  to  $\delta^{11}\text{B}_{\text{borate}}$  (eg.  $\Delta\delta^{11}\text{B}_{\text{carbonate}}/\Delta\delta^{11}\text{B}_{\text{borate}}$ ) in core-  
56 tops is consistent with previous studies for *T. sacculifer* and *G. ruber* and close to unity for *N. dutertrei*, *O. universa*  
57 and combined deep-dwelling species. Deep-dwelling species closely follow the core-top calibration for *O.*  
58 *universa*, which is attributed to respiration-driven microenvironments likely caused by light limitation and/or  
59 symbiont/host interactions. Our data support the premise that utilizing boron isotope measurements of multiple  
60 species within a sediment core can be utilized to constrain vertical profiles of pH and  $\text{pCO}_2$  at sites spanning  
61 different oceanic regimes, thereby constraining changes in vertical pH gradients and yielding insights into the past  
62 behavior of the oceanic carbon pumps.

## 63 1. Introduction

64 The oceans are absorbing a substantial fraction of anthropogenic carbon emissions resulting in declining  
65 surface ocean pH (IPCC, 2014). Yet there is a considerable uncertainty over the magnitude of future pH change in  
66 different parts of the ocean and the response of marine biogeochemical cycles to physio-chemical parameters (T,  
67 pH) caused by climate change (Bijma et al., 2002; Ries et al., 2009). Therefore, there is an increased interest in  
68 reconstructing past seawater pH (Hönisch and Hemming, 2004; Liu et al., 2009; Wei et al., 2009; Douville et al.,  
69 2010), in understanding spatial variability in aqueous pH and carbon dioxide ( $p\text{CO}_2$ ) (Foster et al., 2008; Martinez-  
70 Boti et al., 2015b; Raitzsch et al., 2018), and in studying the response of the biological carbon pump using  
71 geochemical proxies (Yu et al., 2007, 2010, 2016).

72 Although all proxies for carbon cycle reconstruction are complex in nature (Pagani et al., 2005; Tripathi et  
73 al., 2009, 2011; Allen and Hönisch, 2012), the boron isotope composition of foraminiferal tests (expressed as  
74  $\delta^{11}\text{B}_{\text{carbonate}}$ ) is emerging as one of the more robust available tools (Ni et al., 2007; Foster et al., 2008, 2012; Henehan  
75 et al., 2013; Martinez-Boti et al., 2015b; Chalk et al., 2017). The study of laboratory-cultured foraminifera has  
76 demonstrated a systematic dependence of the boron isotope composition of tests on solution pH (Sanyal et al.,  
77 1996, 2001; Henehan et al., 2013, 2016). Core-top measurements on globally distributed samples also show a  
78 boron isotope ratio sensitivity to pH with taxa-specific offsets from the theoretical fractionation line of borate ion  
79 (Rae et al., 2011; Henehan et al., 2016; Raitzsch et al., 2018).

80 Knowledge of seawater pH, in conjunction with constraints on one other carbonate system parameter  
81 (Total Alkalinity (TA), DIC (dissolved inorganic carbon),  $[\text{HCO}_3^-]$ ,  $[\text{CO}_3^{2-}]$ ), can be utilized to constrain aqueous  
82  $p\text{CO}_2$ . Application of empirical calibrations for boron isotope ratio, determined for select species of foraminifera  
83 from core-tops and laboratory cultures, has resulted in accurate reconstructions of  $p\text{CO}_2$  utilizing downcore  
84 samples from sites that are currently in quasi-equilibrium with the atmosphere at present. Values of  $p\text{CO}_2$   
85 reconstructed from planktonic foraminifera boron isotope ratios are analytically indistinguishable from ice core  
86  $\text{CO}_2$  records (Foster et al., 2008; Henehan et al., 2013; Chalk et al., 2017).

87 The last decade has produced several studies aiming at reconstructing past seawater pH using boron  
88 isotopes to constrain atmospheric  $p\text{CO}_2$  in order to understand the changes in the global carbon cycle (Hönisch et  
89 al., 2005, 2009; Foster et al., 2008, 2012, 2014; Seki et al., 2010; Bartoli et al., 2011; Henehan et al., 2013;  
90 Martinez-Boti et al., 2015a, 2015b; Chalk et al., 2017). In addition to reconstructing atmospheric  $p\text{CO}_2$ , the boron  
91 isotopes proxy has been applied to mixed-layer planktonic foraminifera at sites out of equilibrium with the  
92 atmosphere to constrain past air-sea fluxes (Foster et al., 2014; Martinez-Boti et al., 2015b). A small body of work  
93 has examined whether data for multiple species in core-top (Foster et al., 2008) and down-core samples could be  
94 used to constrain vertical profiles of pH through time (Palmer et al., 1998; Pearson and Palmer, 1999; Anagnostou  
95 et al., 2016).

96 Here we add to the emerging pool of boron isotope data in planktonic foraminifera from different  
97 oceanographic regimes, including data for species that have not previously been examined. We utilize a low-blank  
98 (15 pg B to 65 pg B), high precision (2sd on the international standard JCP-1 is 0.20 ‰, n=6)  $\delta^{11}\text{B}_{\text{carbonate}}$  analysis  
99 method for small samples (down to ~250  $\mu\text{g CaCO}_3$ ), modified after Misra et al. (2014), to study multiple species  
100 of planktonic foraminifera. The studied sediment core-tops span a range of oceanographic regimes, including open-  
101 ocean oligotrophic settings and marginal seas. We constrain calibrations for different species, and compare results  
102 to published work (Foster et al., 2008; Henehan et al., 2013; Henehan et al., 2016; Martinez-Boti et al., 2015b;

103 Raitzsch et al., 2018). We also test whether these data support the application of boron isotope measurements of  
104 multiple species within a sediment core as a proxy for constraining vertical profiles of pH and pCO<sub>2</sub>.

105

## 106 **2. Background**

### 107 **2.1 Planktonic foraminifera as archives of seawater pH**

108 Planktonic foraminifera are used as archives of past environmental conditions within the mixed layer and  
109 thermocline, as their chemical composition is correlated with the physio-chemical parameters of their calcification  
110 environment (Ravelo and Fairbanks, 1992; Elderfield and Ganssen, 2000; Dekens et al., 2002; Anand et al., 2003;  
111 Sanyal et al., 2001; Ni et al., 2007; Henehan et al., 2013, 2015, 2016; Howes et al., 2017; Raitzsch et al., 2018).  
112 The utilization of geochemical data for multiple planktonic foraminifera species with different ecological  
113 preferences to constrain vertical gradients has been explored in several studies. The framework for such an  
114 approach was first developed using modern samples of planktonic foraminifera for oxygen isotopes, where it was  
115 proposed as a tool to constrain vertical temperature gradients and study physical oceanographic conditions during  
116 periods of calcification (Ravelo and Fairbanks, 1992).

117 Because planktonic foraminifera species complete their lifecycle in a particular depth habitat due to their  
118 ecological preference (Ravelo and Fairbanks, 1992; Farmer et al., 2007), it is theoretically possible to reconstruct  
119 water column profiles of pH using boron isotope ratios data from multiple taxa (Palmer and Pearson, 1998;  
120 Anagnostou et al., 2016). The potential use of an analogous approach to reconstruct past profiles of seawater pH  
121 was first highlighted by Palmer and Pearson (1998) on Eocene samples to constrain pH-depth gradients. However,  
122 in these boron isotope-based studies, it was assumed that boron isotope offset from seawater and foraminiferal  
123 carbonate were constant, which is an assumption not supported by subsequent studies (e.g., Hönisch et al., 2003;  
124 Foster et al., 2008; Henehan et al., 2013, 2016; Raitzsch et al., 2018; Rae, 2018). Furthermore, boron isotope ratio  
125 differences between foraminifera species inhabiting waters of the same pH makes the acquisition of more core-  
126 top and culture data essential for applications of the proxy.

127

### 128 **2.2 Boron systematics in seawater**

129 Boron is a conservative element in seawater with a long residence time ( $\tau_B \sim 14$  Myr) (Lemarchand et al.,  
130 2002a). In seawater, boron exists as trigonal boric acid B(OH)<sub>3</sub> and tetrahedral borate ion B(OH)<sub>4</sub><sup>-</sup> (borate). The  
131 relative abundance of boric acid and borate ion is a function of the ambient seawater pH. At standard open ocean  
132 conditions (T = 25 °C and S = 35), the dissociation constant of boric acid is 8.60 (Dickson, 1990), implying that  
133 boron mainly exists in the form of boric acid in seawater. Since the pK<sub>B</sub> and seawater pH (e.g., ~8.1, NBS) values  
134 are similar, it implies that small changes in seawater pH will induce strong variations in the abundance of the two  
135 boron species (Fig. 1).

136 Boron has two stable isotopes, <sup>10</sup>B and <sup>11</sup>B, with average relative abundances of 19.9 and 80.1 %,  
137 respectively. Variations in B isotope ratio are expressed in conventional delta (δ) notation:

138

$$139 \quad \delta^{11}\text{B} (\text{‰}) = 1000 \times \left( \frac{{}^{11}\text{B}/{}^{10}\text{B}_{\text{Sample}}}{{}^{11}\text{B}/{}^{10}\text{B}_{\text{NIST SRM 951}}} - 1 \right) \quad (1)$$

140

141 where positive values represent enrichment in the heavy isotope  $^{11}\text{B}$ , and negative values enrichment in the light  
142 isotope  $^{10}\text{B}$ , relative to the standard reference material. Boron isotope values are reported versus the NIST SRM  
143 951 boric acid standard (Cantazaro et al., 1970).

144  $\text{B}(\text{OH})_3$  is enriched in  $^{11}\text{B}$  compared to  $\text{B}(\text{OH})_4^-$  with a constant offset between the two chemical  
145 species, within the range of physio-chemical variation observed in seawater, given by the fraction factor ( $\alpha$ ). The  
146 fractionation ( $\epsilon$ ) between  $\text{B}(\text{OH})_3$  and  $\text{B}(\text{OH})_4^-$  of  $27.2 \pm 0.6 \text{ ‰}$  has been empirically determined by Klochko et  
147 al. (2006) in seawater. Note, Nir et al. (2015) calculate this fractionation, using an independent method, to be  $26$   
148  $\pm 1 \text{ ‰}$ , which is within the analytical uncertainty of the Klochko et al. (2006) value. We use a fractionation of  $27.2$   
149  $\text{‰}$  determined by Klochko et al. (2006) in this study.

150

### 151 **2.3 Boron isotopes in planktonic foraminifera calcite**

152 Many biogenic carbonate-based geochemical proxies are affected by “vital effects” or biological  
153 fractionations (Urey et al., 1951). The  $\delta^{11}\text{B}_{\text{carbonate}}$  in foraminifera exhibits species-specific offsets (see Rae et al.,  
154 2018 for review) compared to theoretical predictions for the boron isotopic composition of  $\text{B}(\text{OH})_4^-$  (expressed as  
155  $\delta^{11}\text{B}_{\text{borate}}$ ,  $\alpha=1.0272$ , Klochko et al., 2006). As the analytical and technical aspects of boron isotope measurements  
156 have improved (Foster et al., 2008; Rae et al., 2011; Misra et al., 2014; Lloyd et al., 2018), evidence for taxonomic  
157 differences have not been eliminated, but have become increasingly apparent (Foster et al., 2008, 2018; Henehan  
158 et al 2013, 2016; Foster et al., 2016; Rae et al., 2018; Raitzsch et al., 2018).

159 At present, culture and core-top calibrations have been published for several planktonic species including  
160 *Trilobatus sacculifer*, *Globigerinoides ruber*, *Globigerina bulloides*, *Neogloboquadrina pachyderma*, *Orbulina*  
161 *universa* (Foster et al., 2008; Henehan et al., 2013; Henehan et al., 2015; Sanyal et al., 1996; Sanyal et al., 2001).  
162 Although the boron isotopic composition of several species of foraminifera is now commonly used for  
163 reconstructing surface seawater pH, for other species, there is a lack of data constraining the sensitivity of boron  
164 isotopes in foraminiferal carbonate and borate ion in seawater.

165

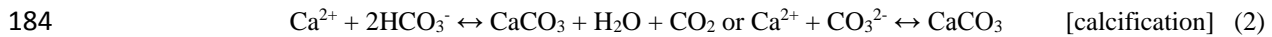
### 166 **2.4 Origin of biological fractionations in foraminifera**

167 Perforate foraminifera are calcifying organisms that maintain a large degree of biological control over  
168 their calcification space, and thus, mechanisms of biomineralization may be of significant importance in  
169 controlling the  $\delta^{11}\text{B}$  of the biogenic calcite. The biomineralization of foraminifera is based on seawater  
170 vacuolization (Erez, 2003; de Nooijer et al., 2014) with parcels of seawater being isolated by an organic matrix  
171 thereby creating a vacuole filled with seawater. Recent work has also demonstrated that even if the chemical  
172 composition of the reservoirs is modified by the organism, seawater is directly involved in the calcification process  
173 with vacuoles formed at the periphery of the shell (de Nooijer et al., 2014). Culture experiments by Rollion-Bard  
174 and Erez (2010) have proposed that the pH at the site of biomineralization is elevated to an upper pH limit of  $\sim 9$   
175 for the shallow-water, symbiont-bearing benthic foraminifera *Amphistegina lobifera*, which would support a pH  
176 modulation of a calcifying fluid in foraminifera. The extent to which these results apply to planktonic foraminifera  
177 is not known, although pH modulation of calcifying fluid may influence the  $\delta^{11}\text{B}$  of planktonic foraminifera.

178 For taxa with symbionts, the microenvironment surrounding the foraminifera is chemically different from  
179 seawater due to photosynthetic activity (Jorgensen et al., 1985; Rink et al., 1998; Köhler-Rink and Kühl, 2000).  
180 Photosynthesis by symbionts elevates the pH of microenvironments (Jorgensen et al., 1985; Rink et al., 1998;

181 Wolf-Gladrow et al., 1999; Köhler-Rink and Kühl, 2000), while calcification and respiration decrease  
182 microenvironment pH (Equation 2 and 3).

183



186

187  $\delta^{11}\text{B}$  in foraminifera is primary controlled by seawater pH, but also depends on the pH alteration of  
188 microenvironments due to calcification, respiration and symbiont photosynthesis.  $\delta^{11}\text{B}_{\text{carbonate}}$  should therefore  
189 reflect the relative dominance of these processes and may account for species-specific  $\delta^{11}\text{B}$  offsets. Theoretical  
190 predictions from Zeebe et al. (2003) and foraminiferal data from Hönisch et al. (2003) explored the influence of  
191 microenvironment pH in  $\delta^{11}\text{B}$  signature of foraminifera. Their work also suggested that for a given species, there  
192 should be a constant offset observed between the boron isotope composition of foraminifera and borate ion over a  
193 large range of pH, imparting confidence in utilizing species-specific boron isotope data as a proxy for seawater  
194 pH.

195 Comparison of boron isotope data for multiple planktonic foraminiferal species indicate that taxa with  
196 high levels of symbiont activity such as *T. sacculifer* and *G. ruber* show higher  $\delta^{11}\text{B}$  values than the  $\delta^{11}\text{B}$  of ambient  
197 borate (Foster et al., 2008, Henehan et al., 2013, Raitzsch et al., 2018). The sensitivities ( $\Delta\delta^{11}\text{B}_{\text{carbonate}}/\Delta\delta^{11}\text{B}_{\text{borate}}$ ,  
198 hereafter referred to as the slope) of existing calibrations suggest a different species-specific sensitivity for these  
199 species compared to other taxa (Sanyal et al., 2001; Henehan et al., 2013; Henehan et al., 2015; Raitzsch et al.,  
200 2018). For example, *Orbulina universa* exhibits a lower  $\delta^{11}\text{B}$  than *in situ*  $\delta^{11}\text{B}$  values of borate ion (Henehan et  
201 al., 2016), consistent with the species living deeper in the water column characterized by reduced photosynthetic  
202 activity.

203 It is possible that photosynthetic activity by symbionts might not be able to compensate for changes in  
204 calcification and/or respiration, leading to an acidification of the microenvironment. It is interesting to note that  
205 for *O. universa* the slope determined for the field-collected samples is not statistically different from unity ( $0.95 \pm$   
206  $0.17$ ) (Henehan et al. 2016), while culture experiments report slopes of  $\leq 1$  for multiple species including *G. ruber*  
207 (Henehan et al., 2013), *T. sacculifer* (Sanyal et al., 2001), and *O. universa* (Sanyal et al., 1999). More core-top and  
208 culture calibrations are needed to refine those slopes and understand if significant differences are observed, which  
209 is part of the motivation for this study.

210

## 211 **2.5 Planktic foraminifera depth and habitat preferences**

212 The preferred depth habitat of different species of planktonic foraminifera depends on their ecology,  
213 which in turn is dependent on hydrographic conditions. For example, *G. ruber* is commonly found in the mixed  
214 layer (Fairbanks and Wiebe, 1980; Dekens et al., 2002; Farmer et al., 2007) during the summer (Deuser et al.,  
215 1981) whereas *T. sacculifer* is present in the mixed layer until mid-thermocline depths (Farmer et al., 2007) during  
216 spring and summer (Deuser et al., 1981, 1989). Specimens of *P. obliquiloculata* and *N. dutertrei* are abundant  
217 during winter months (Deuser et al., 1989), with an acme in the mixed layer (~60m) for *P. obliquiloculata* and at  
218 mid-thermocline depths for *N. dutertrei* (Farmer et al., 2007). In contrast, *O. universa* tends to record annual  
219 average conditions within the mixed layer. Specimens of *G. menardii* calcify within the seasonal thermocline  
220 (Fairbanks et al., 1982, Farmer et al., 2007, Regenberg et al., 2009), and in some regions in the upper thermocline

221 (Farmer et al., 2007), and records annual temperatures. *G. tumida* is found at the lower thermocline or below the  
222 thermocline and records annual average conditions (Fairbanks and Wiebe, 1980; Farmer et al., 2007, Birch et al.,  
223 2013). Although the studies listed above showed evidence for species-specific living depth-habitat affinities, recent  
224 direct observations showed that environmental conditions (e.g. temperature, light) was locally responsible for the  
225 variability in the living depth of certain foraminifera species in the eastern North Atlantic (Rebotim et al., 2017).  
226

### 227 3. Materials and Methods

#### 228 3.1 Localities studied 229

230 Core-top locations were selected to span a broad range of seawater pH, carbonate system parameters, and  
231 oceanic regimes. Samples from Atlantic Ocean (CD107-A), Indian Ocean (FC-01a and FC-02a), Arabian Sea  
232 (FC-13a and FC-12b) and Pacific Ocean (WP07-01, A14, and Ocean Drilling Program 806A and 807A) were  
233 analyzed; characteristics of the sites are summarized in Table 1 and S7, Fig. 2, and Fig. 3.

234 Atlantic site CD107-a (CD107 site A) was cored in 1997 by the Benthic Boundary Layer program  
235 (BENBO) (K.S. Black et al., 1997 - cruise report RRS Charles Darwin Cruise 107). Arabian Sea sites FC-12b  
236 (CD145 A150) and FC-13a (CD145 A3200) were retrieved by the *Charles Darwin* in the Pakistan Margin in 2004  
237 (B.J. Bett et al., 2003 - cruise report n°50 RRS Charles Darwin Cruise 145). A14 was recovered by box corer in  
238 the southern area of the South China Sea in 2012. Core WP07-01 was obtained from the Ontong Java Plateau using  
239 a giant piston corer during the Warm Pool Subject Cruise in 1993. Holes 806A and 807A were retrieved on Leg  
240 130 by the Ocean Drilling Program (ODP). The top 10 cm of sediment from CD107-A have been radiocarbon  
241 dated to be Holocene <3 ky (Thomson et al., 2000). Samples from multiple box cores from Indian Ocean sites  
242 were radiocarbon dated as Holocene <7.3 ky (Wilson et al., 2012). Samples from western equatorial Pacific Site  
243 806B, close to site WP07-01, are dated to between 7.3-8.6 ky (Lea et al., 2000). Arabian Sea and Pacific core-top  
244 samples were not radiocarbon dated but are assumed to be Holocene.  
245

#### 246 3.2 Species

247 Around 50-100 foraminifera shells were picked from the 400-500 µm fraction size for *Globorotalia*  
248 *menardii* and *Globorotalia tumida*, >500 µm for *Orbulina universa*, and from the 250-400 µm fraction size for  
249 *Trilobatus sacculifer* (w/o sacc, without sacc-like final chamber), *Trilobatus sacculifer* (sacc, sacc-like final  
250 chamber), *Globigerinoides ruber* (white, sensu stricto), *Neogloboquadrina dutertrei*, and *Pulleniatina*  
251 *obliquiloculata*. The samples picked for analyses were visually well preserved.  
252

#### 253 3.3 Sample cleaning

254 Briefly, picked foraminifera were gently cracked open, clay removed with successive ultrasonication  
255 steps in MQ water and methanol and then were checked for coarse-grained silicates. The next stages of sample  
256 processing and chemical separation were performed in a class 1000 clean lab equipped with boron-free HEPA  
257 filters. Samples were cleaned using full reductive and oxidative cleaning (Boyle, 1981; Boyle and Keigwin, 1985;  
258 Barker et al., 2003). Samples from the South China Sea (sites A14, E035) presented high Mn and high Fe. Due to  
259 potential Fe-Mn oxide and hydroxides the reductive cleaning was used. Previous comparisons of cleaning methods  
260 have shown there is no impact of the reductive step on B/Ca (Misra et al., 2014b) but there is an impact of the  
261 reductive step on Mg/Ca (Barker et al., 2003 and others), nevertheless, it is possible that Fe-Mn oxide and

262 hydroxides can result in non-negligible Mg and B contamination. Because this study was designed to investigate  
263 boron proxies and in order to be consistent in methodology, the reductive cleaning was used at all sites. Cleaned  
264 samples selected for this study did not yield high Mn concentrations (see supplement for discussion on  
265 contamination).

266 A final leaching step with 0.001N HCl was done before dissolution in 1N HCl. Hydrochloric acid was  
267 used to allow complete dissolution of the sample including Fe-Mn oxide and hydroxides if present. Each sample  
268 was divided into two aliquots: an aliquot for boron purification and one aliquot for trace element analysis.

269

### 270 **3.4 Reagents**

271 Double-distilled HNO<sub>3</sub> and HCl acids (from Merck® grade) and a commercial bottle of HF Ultrapure  
272 grade were used at Brest. Double-distilled acids were used at Cambridge. All acids and further dilutions were  
273 prepared using double-distilled 18.2 MΩ.cm<sup>-1</sup> MQ water. Working standards for isotope ratio and trace element  
274 measurements were freshly diluted on a daily basis with the same acids used for sample preparation to avoid any  
275 matrix effects.

276

### 277 **3.5 Boron isotopes**

278 Boron purification for isotopic measurement was done utilizing microdistillation method developed by  
279 Gaillardet et al. (2001), for Ca-rich matrices by Wang et al. (2010) and adapted at Cambridge by Misra et al.  
280 (2014a). 70 μL of carbonate sample dissolved in 1N HCl was loaded on a cap of a clean fin legged 5 mL conical  
281 beaker upside down. The tightly closed beaker was put on a hotplate at 95°C for 15 hours. The beakers were taken  
282 off the hotplate and were allowed to cool for 15 min. The cap where the residue formed was replaced by a clean  
283 one. Then, 100 μL of 0.5% HF were added to the distillate.

284 Boron isotopic measurements were carried out on a Thermo Scientific ®Neptune+ MC-ICP-MS at the  
285 University of Cambridge. Neptune+ was equipped with Jet interface and two 10<sup>13</sup> Ω resistors. The instrumental  
286 setup included Savillex® 50μl/min C-flow self-aspirating nebulizer, single pass Teflon® Scott-type spray chamber  
287 constructed utilizing Savillex® column components, 2.0 mm Pt injector from ESI®, Thermo® Ni ‘normal’ type  
288 sample cone and ‘X’ type skimmer cones. Both isotopes of boron were determined utilizing 10<sup>13</sup> Ω resistors (Misra  
289 et al., 2014a; Lloyd et al., 2018).

290 The sample size for boron isotope analyses typically ranged from 10 ppb B (~5 ng B) to 20 ppb B samples  
291 (~10 ng B). Instrumental sensitivity for <sup>11</sup>B was 17 mV/ppb B (eg. 170 mV for 10ppb B) in wet plasma at 50μl/min  
292 sample aspiration rate. Intensity of <sup>11</sup>B for a sample at 10ppb B was typically 165mV ± 5mV, which closely  
293 matched the 170mV ± 5mV of the standard. Due to the low boron content of the samples extreme care was taken  
294 to avoid boron contamination during sample preparation and reduce memory effect during analysis. Procedural  
295 boron blanks ranged from 15pg B to 65 pg B and contributed to less than <1% of the sample signal. The acid blank  
296 during analyses was measured at ≤ 1mV on <sup>11</sup>B, meaning a contribution < 1% of the sample intensity, no memory  
297 effect was observed within and across sessions. No matrix effect resulting from the mix HCl/HF was observed on  
298 the δ<sup>11</sup>B.

299 Analyses of external standards were done to ensure data quality. For δ<sup>11</sup>B measurements one carbonate  
300 standard and one coral were utilized: the JcP-1 (Geological Survey of Japan, Tsukuba, Japan) international  
301 standard (Gutjahr et al., 2014) and the NEP coral (Porites sp., δ<sup>11</sup>B = 26.12 ± 0.92 ‰, 2SD, n=33 Holcomb et al.,



2015 and Sutton et al., 2018, Table S2) from University of Western Australia/Australian National University. A certified boric acid standard, the ERM<sup>®</sup> AE121 ( $\delta^{11}\text{B} = 19.9 \pm 0.6 \text{ ‰}$ , SD, certified) was used to monitor reproducibility and drift during each session (Vogl and Rosner, 2011; Foster et al., 2013; Misra et al., 2014). Results for the isotopic composition of the NEP coral are shown in Table S2, average values are  $\delta^{11}\text{B}_{\text{NEP}} = 25.70 \pm 0.93 \text{ ‰}$  (2SD, n=22) over different 7 analytical sessions with each number representing an ab-initio processed sample. Our results are within error of published values of  $26.20 \pm 0.88 \text{ ‰}$  (2SD, n = 27) and  $25.80 \pm 0.89 \text{ ‰}$  (2SD, n = 6) by Holcomb et al. (2015) and Sutton et al. (2018) respectively. Chemically cleaned JCp-1 samples were measured at  $24.06 \pm 0.20$  (2SD, n=6) and is within error of published values of  $24.37 \pm 0.32 \text{ ‰}$ ,  $24.11 \pm 0.43 \text{ ‰}$  and  $24.42 \pm 0.28 \text{ ‰}$  by Holcomb et al. (2015), Farmer et al. (2016) and Sutton et al. (2018) respectively.

311

### 312 3.6 Trace elements

313 The calcium concentration of each sample was measured on an ICP-AES <sup>®</sup> Ultima 2 HORIBA at the  
314 Pôle spectrometrie Océan (PSO), UMR6538 (Plouzané, France). Samples were then diluted to fixed calcium  
315 concentrations (typically 10 ppm or 30 ppm Ca) using 0.1 M HNO<sub>3</sub> & 0.3 M HF matching multi-element standards  
316 Ca concentration to avoid any matrix effects (Misra et al., 2014b). Levels of remaining HCl (<1%) in these diluted  
317 samples were negligible and did not contribute to matrix effects. Trace elements (e.g. X/Ca ratios) were analyzed  
318 on a Thermo Scientific <sup>®</sup> Element XR HR-ICP-MS at the PSO, Ifremer (Plouzané, France).

319 Trace element analyses were done at a Ca concentration of 10 or 30 ppm. The typical blanks for a 30 ppm  
320 Ca session were: <sup>7</sup>Li < 2%, <sup>11</sup>B < 7%, <sup>25</sup>Mg < 0.2% and <sup>43</sup>Ca < 0.02%. Additionally, blanks for a 10 ppm Ca session  
321 were: <sup>7</sup>Li < 2.5%, <sup>11</sup>B < 10%, <sup>25</sup>Mg < 0.4% and <sup>43</sup>Ca < 0.05%. Due to strong memory effect for boron and  
322 instrumental drift on the Element XR, long sessions of conditioning were done prior analyses. Boron blanks were  
323 driven below 5% of signal intensity usually after 4 to 5 days of continuous analyses of carbonate samples. External  
324 reproducibility was determined on the consistency standard Cam-Wuellestorf (courtesy of the University of  
325 Cambridge) (Misra et al., 2014b), Table S3. Our X/Ca ratio measurements on the external standard Cam-  
326 Wuellestorf were all the time within error of the published value (Table S3) validating the robustness of our trace  
327 elements data. Analytical uncertainty of a single measurement was calculated from the reproducibility of the Cam-  
328 Wuellestorf, measured during a particular mass spectrometry session. The analytical uncertainties (2SD, n=31,  
329 Table S3) on the X/Ca ratios are:  $\pm 0.4 \text{ } \mu\text{mol/mol}$  for Li/Ca,  $\pm 7 \text{ } \mu\text{mol/mol}$  for B/Ca and  $\pm 0.01 \text{ mmol/mol}$  for Mg/Ca  
330 respectively.

331

### 332 3.7 Oxygen isotopes

333 Carbonate  $\delta^{13}\text{C}$  and  $\delta^{18}\text{O}$  were measured on a Gas Bench II coupled to a Delta V mass spectrometer at the  
334 stable isotope facility of Pôle spectrometrie Océan (PSO), Plouzané. Around 20 shells were weighed, crushed and  
335 clay removed following the same method described in section 3.3 (Barker et al., 2003). The recovered foraminifera  
336 were weighed in tubes and flushed with He gas. Samples were then digested in phosphoric acid and analyzed.  
337 Results were calibrated to the VPDB scale by international standard NBS19 and analytical precision on the in-  
338 house standard Ca21 was better than  $\pm 0.11 \text{ ‰}$  for  $\delta^{18}\text{O}$  (1SD, n=5) and  $\pm 0.03 \text{ ‰}$  for  $\delta^{13}\text{C}$  (1SD, n=5).

339

### 340 3.8 Calcification depth determination

341 We utilized two different chemo-stratigraphic methods to estimate the calcification depth (CD) in this  
342 study (Table S6 and S7). The first method (CD1), commonly used in paleoceanography, utilizes  $\delta^{18}\text{O}$   
343 measurements of the carbonate ( $\delta^{18}\text{O}_c$ ) to estimate calcification depths (referred to as  $\delta^{18}\text{O}$ -based calcification  
344 depths) (Schmidt et al., 2002; Mortyn et al., 2003; Sime et al., 2005; Farmer et al., 2007; Birsh et al., 2013).  
345 Rebotim et al. (2017) also showed good correspondence between living depth habitat and calcification depth  
346 derived using CD1. The second method (CD2) utilizes Mg/Ca-based temperature estimates ( $T_{\text{Mg/Ca}}$ ) to constrain  
347 calcification depths (Quintana Krupinski et al., 2017). However, we note that reductive cleaning leads to a decrease  
348 in Mg/Ca that in turn would result in a bias towards deeper calcification depths, which is not the case when we  
349 utilize non-Mg/Ca-based methodologies. In both cases, the prerequisite was that vertical profiles of seawater  
350 temperature are available for different seasons in ocean atlases and cruise reports, and that hydrographic data and  
351 geochemical proxy signatures can be compared to assess the depth in the water column that represents the taxon's  
352 maximum abundance.

353 Because both methods have their uncertainties (in one case, use of taxon-specific calibrations, and in the  
354 other, analytical limitations), both estimates of calcification depth were compared to published values for the basin  
355 (CD3), and where available, for the same site (Table S6). To select which calcification depth to use for further  
356 calculations, we first looked at CD<sub>1</sub>, CD<sub>2</sub> and CD<sub>3</sub>. If, CD<sub>1</sub> and CD<sub>2</sub> were similar we selected this calcification  
357 depth, if CD<sub>1</sub> and CD<sub>2</sub> were different we chose literature values, CD<sub>3</sub>, when available. For some less studied  
358 species, like *G. tumida*, *G. menardii* or *P. obliquiloculata*, CD<sub>3</sub> was not always available but when available  
359 showed good correspondence with our CD<sub>2</sub>, moreover due to availability of Mg/Ca-temperature taxon-specific  
360 calibrations we preferentially use CD<sub>2</sub> for those species.

361 We applied (based on uncertainties of our measurements) an uncertainty of  $\pm 10\text{m}$  for calcification depths  
362  $> 70\text{ m}$  and an uncertainty of  $\pm 20\text{ m}$  when calcification depths  $< 70\text{ m}$ . Direct observations of living depths of  
363 foraminifera remain limited. However, the depth uncertainties reported here are in line with the uncertainties  
364 calculated based on direct observations in the eastern North Atlantic which give a standard error on average living  
365 depths ranging from 6-22 m for the same species (Rebotim et al., 2017). The decrease in Mg/Ca due to reductive  
366 cleaning was not taking into account, because it has not been studied for most of the species used in this study and  
367 because the depth uncertainty applied based on  $\delta^{18}\text{O}$  analytical error is conservative relative to the uncertainty of  
368 a 10% decrease in Mg/Ca equivalent that would be equivalent to  $\sim 1.2^\circ\text{C}$ . The depth habitats utilized to derive *in*  
369 *situ* parameters are summarized in Table S7.

370

### 371 3.9 $\delta^{11}\text{B}_{\text{borate}}$

372 Two carbonate system parameters are needed to fully constrain the carbonate system. Following the  
373 approach of Foster et al., (2008) we used the GLODAP database (Key et al., 2004) corrected for anthropogenic  
374 inputs in order to estimate pre-industrial carbonate system parameters at each site. Temperature, salinity and  
375 pressure for each site are from the World Ocean Database 2013 (Boyer et al., 2013). We utilized the R<sup>®</sup> code in  
376 Henehan et al, (2016) (courtesy of Michael Henehan) to calculate the  $\delta^{11}\text{B}_{\text{borate}}$ ,  $\delta^{11}\text{B}_{\text{borate}}$  uncertainty and derive  
377 our calibrations. Uncertainty for  $\delta^{11}\text{B}_{\text{borate}}$  utilizing Henehan's code was similar to uncertainty calculated by  
378 applying 2 standard deviations of the  $\delta^{11}\text{B}_{\text{borate}}$  profiles within the limits imposed by our calcification depth.

379 The Matlab<sup>®</sup> template provided by Zeebe and Wolf-Gladow, (2001) was used to calculate pCO<sub>2</sub> from  
380 TA; temperature, salinity and pressure were included in the calculations. Total boron was calculated from Lee et  
381 al., (2010), K<sub>1</sub> and K<sub>2</sub> were calculated from Mehrbach et al. (1973) refitted by Dickson and Millero (1987).

382 Statistical tests were made utilizing GraphPad<sup>®</sup> software, linear regressions for calibration were derived  
383 utilizing R<sup>®</sup> code in Henehan et al, (2016) (courtesy of Michael Henehan) with k (number of wild bootstrap  
384 replicates) equal to 500.

385

## 386 4. Results

387

### 388 4.1 Depth habitat

389 The calcification depths utilized in this paper are summarized in Tables S6 and S7, including a comparison  
390 of calcification depth determination methods. The calculated calcification depths are consistent with the ecology  
391 of each species and the physical properties of the water column of the sites. Specimens of *G. ruber* and *T. sacculifer*  
392 appear to be living in the shallow mixed layer (0-100 m), with *T. sacculifer* living or migrating deeper than *G.*  
393 *ruber* (down to 125 m). Specimens of *O. universa* and *P. obliquiloculata* are living in the upper thermocline; *G.*  
394 *menardii* is found in the upper thermocline until the thermocline depth specific to the location; *N. dutertrei* is living  
395 near thermocline depths and *G. tumida* is found in the lower thermocline.

396 Data from the multiple approaches for calculating calcification depth (CD1, CD2 and CD3) implies that  
397 some species inhabit deeper environments in the Western Equatorial Pacific (WEP) relative to the Arabian Sea,  
398 which in turn are deeper-dwelling than the same morpho-species occurring in the Indian Ocean. In some cases, we  
399 find evidence for differences in habitat depth of up to ~100m between the WEP and the Arabian Sea. This trend is  
400 observed for *G. ruber* and *T. sacculifer*, but not for *O. universa*.

401 Some differences are observed between the two methods for calcification depth determination that are  
402 based on  $\delta^{18}\text{O}$  and Mg/Ca (CD1 and CD2, respectively). These differences might be due to the choice of  
403 calibration. Alternatively, our uncertainties for  $\delta^{18}\text{O}$  implies larger uncertainties on calcification depth  
404 determinations that use this approach, compared to Mg/Ca based estimates.

405

### 406 4.2 Empirical calibrations of foraminiferal $\delta^{11}\text{B}_{\text{carbonate}}$ to $\delta^{11}\text{B}_{\text{borate}}$

407 Results for the different species analyzed in this study are presented in Fig. 4, Fig. 5 and summarized in  
408 Table 2; additionally, published calibrations for comparison are summarized in Table 3.

409

#### 410 4.2.1 *G. ruber*

411 Samples were picked from the 250-300  $\mu\text{m}$  fraction, except for the WEP sites where *G. ruber* shells were  
412 picked from the 250-400  $\mu\text{m}$  fraction. Weight per shell averaged  $11 \pm 4 \mu\text{g}$  (n=4, SD) although the weight was not  
413 measured on the same sub-sample analyzed for  $\delta^{11}\text{B}$  and trace elements or at the WEP sites. In comparison to  
414 literature, the size fraction used for this study was smaller: Foster et al. (2008) used the 300-355 $\mu\text{m}$  fraction,  
415 Henehan et al. (2013) utilized multiple size fractions (250-300, 250-355, 300-355, 355-400 and 400-455  $\mu\text{m}$ ) and  
416 Raitzsch et al. (2018) used the 315-355  $\mu\text{m}$  fraction.

417 Our results for *G. ruber* (Fig. 4) are in close agreement with published data from other core-tops, sediment  
418 traps, tows, and culture experiments for  $\delta^{11}\text{B}_{\text{borate}} > 19 \text{‰}$  (Foster et al., 2008, Henehan et al., 2013, Raitzsch et al.,

419 2018). However, the two datapoints from  $\delta^{11}\text{B}_{\text{borate}} < 19 \text{ ‰}$  are lower compared to previous studies. Elevated  
420  $\delta^{11}\text{B}_{\text{carbonate}}$  values relative to  $\delta^{11}\text{B}_{\text{borate}}$  has been explained by the high photosynthetic activity of symbionts  
421 (Hönisch et al., 2003; Zeebe et al., 2003). Three calibrations have been derived (Table 3). Linear regression on our  
422 data alone yields a slope of  $1.12 (\pm 1.67)$ . The uncertainty is significant given limited data in our study, and given  
423 this large uncertainty, our sensitivity of  $\delta^{11}\text{B}_{\text{carbonate}}$  to  $\delta^{11}\text{B}_{\text{borate}}$  is also consistent with the low sensitivity trend of  
424 culture experiments from Sanyal et al. (2001) or Henehan et al. (2013). The second calibration made compiling all  
425 data from literature shows a sensitivity similar (e.g.  $0.46 (\pm 0.34)$ ) to the one recently published by Raitzsch et al.,  
426 (2018) (e.g.  $0.45 (\pm 0.16)$ , Table 3). The third linear regression made only on data from the 250-400  $\mu\text{m}$  fraction  
427 from our study and from the 250-300  $\mu\text{m}$  from Henehan et al. (2013) yields a sensitivity of  $0.58 (\pm 0.91)$  similar to  
428 culture experiments from Henehan et al., (2013) (e.g.  $0.6 (\pm 0.16)$ , Table 3). This third calibration is offset by  $\sim$   
429  $0.4 \text{ ‰}$  ( $p > 0.05$ ) compared to culture calibration from Henehan et al. (2013).

430

#### 431 **4.2.2 *T. sacculifer***

432  $\delta^{11}\text{B}_{\text{carbonate}}$  results for *T. sacculifer* (sacc and w/o sacc) (Fig. 4) are compared to published data (Foster et  
433 al., 2008; Martinez-Boti et al., 2015b, Raitzsch et al., 2018). Results for *T. sacculifer* are in good agreement with  
434 the literature and exhibit higher  $\delta^{11}\text{B}_{\text{carbonate}}$  compared to expected  $\delta^{11}\text{B}_{\text{borate}}$  at their collection location. A linear  
435 regression through our data alone yields a slope of  $1.3 \pm 0.2$  but is not statistically different to the results from  
436 Martinez-Boti et al. (2015b) (Table 3), ( $p > 0.05$ ). However, when compiled with published data using the bootstrap  
437 method a slope of  $0.83 \pm 0.48$  is calculated, with a large uncertainty given the variability in the data. It is also  
438 noticeable that *T. sacculifer* (w/o sacc) samples from the WEP have a  $\delta^{11}\text{B}_{\text{carbonate}}$  close to expected  $\delta^{11}\text{B}_{\text{borate}}$  and  
439 are significantly lower compared to the combined *T. sacculifer* of other sites ( $p = 0.01$ , unpaired t-test). When  
440 regressing data from the 250-400  $\mu\text{m}$  fraction, our results are not significantly different from the regression through  
441 data that combine all size fractions (Fig. 4).

442

#### 443 **4.2.3 *O. universa* and deeper-dwelling species: *N. dutertrei*, *P. obliquiloculata*, *G. menardii* and *G. tumida***

444 Our results for *O. universa* (Fig. 4), *N. dutertrei*, *P. obliquiloculata*, *G. menardii* and *G. tumida* (Fig. 5)  
445 exhibit lower  $\delta^{11}\text{B}_{\text{carbonate}}$  compared to the expected  $\delta^{11}\text{B}_{\text{borate}}$  at their collection location. These data for *O. universa*  
446 are not statistically different from the Henehan et al. (2016) calibration ( $p > 0.05$ ). Our results for *N. dutertrei*  
447 expand upon the initial measurements presented in Foster et al. (2008). The different environments experienced  
448 by *N. dutertrei* in our study permit us to extend the range and derive a calibration for this species; the slope is close  
449 to unity ( $0.93 \pm 0.55$ ), and is not significantly different ( $p > 0.05$ ) from the *O. universa* calibration previously  
450 reported by Henehan et al. (2016) (e.g.  $0.95 \pm 0.17$ ). The data for *P. obliquiloculata* exhibits the largest offset from  
451 the theoretical line. The range of  $\delta^{11}\text{B}_{\text{borate}}$  from the samples we have of *G. menardii* and *G. tumida* is not sufficient  
452 to derive calibrations, but the  $\delta^{11}\text{B}_{\text{carbonate}}$  measured for those species are in good agreement with the *N. dutertrei*  
453 calibration and Henehan et al. (2016) calibration for *O. universa*.

454 For *O. universa* and all deep-dwelling species, the slopes are not statistically different from Henehan et  
455 al. (2016) ( $p > 0.05$ ) and are close to unity. If data for deep-dwelling foraminiferal species are pooled together with  
456 each other and with data from Henehan et al. (2016) and Raitzsch et al. (2018), we calculate a slope of  $0.95 (\pm 0.13)$   
457 ( $R^2 = 0.7987$ ,  $p < 0.0001$ ); if only our data are used, we calculate a slope that is not significantly different ( $0.82 \pm$   
458  $0.27$ ;  $p < 0.05$ ).

459

#### 460 4.2.4 Comparison of core-top and culture data

461 The data for *G. ruber* and *T. sacculifer* from the core-tops we measured are broadly consistent with  
462 previous published results. The calibrations between these core-top derived estimates and culture experiments are  
463 not statistically different due to small datasets and uncertainties on the linear regressions (Henehan et al., 2013;  
464 Marinez-Boti et al., 2015; Raitzsch et al., 2018; Table 3). The sensitivities of the species analyzed are not  
465 statistically different and are close to unity.

466

#### 467 4.3 B/Ca ratios

468 B/Ca ratios are presented in Table 2 and Fig. 6. B/Ca data are species-specific and consistent with previous  
469 work (e.g., compiled in Henehan et al., 2016) with ratios higher for *G. ruber* > *T. sacculifer* (sacc) > *T. sacculifer*  
470 (w/o sacc) > *P. obliquiloculata* > *O. universa* > > *G. menardii* > *N. dutertrei* > *G. tumida* > *G. inflata* > *N.*  
471 *pachyderma* > *G. bulloides* (Fig. 6). This study supports species-specific B/Ca ratios as previously published (Yu  
472 et al., 2007; Tripathi et al., 2009, 2011; Allen and Hönisch, 2012; Henehan et al., 2016). Differences between  
473 surface- and deep-dwelling foraminifera are observed, with lower values and a smaller range for the deeper-  
474 dwelling taxa (58-126  $\mu\text{mol/mol}$  vs 83-190  $\mu\text{mol/mol}$  for shallow dwellers), however, the trend for the surface-  
475 dwellers can also be driven by interspecies B/Ca variability. The B/Ca data for deep-dwelling taxa exhibits a  
476 significant correlation with  $[\text{B}(\text{OH})_4^-]/[\text{HCO}_3^-]$  ( $p < 0.05$ ), but no correlation with  $\delta^{11}\text{B}_{\text{carbonate}}$  and temperature (Fig.  
477 S3). Surface-dwelling species have B/Ca ratios that exhibit significant correlations with  $[\text{B}(\text{OH})_4^-]/[\text{HCO}_3^-]$ ,  
478  $\delta^{11}\text{B}_{\text{carbonate}}$  and temperature. The sensitivity of B/Ca to  $[\text{B}(\text{OH})_4^-]/[\text{HCO}_3^-]$  is lower for deep-dwelling species  
479 compared to surface dwelling species. When all the B/Ca data are compiled, significant trends are observed with  
480  $[\text{B}(\text{OH})_4^-]/[\text{HCO}_3^-]$ ,  $\delta^{11}\text{B}_{\text{carbonate}}$  and temperature (Fig. S3). When comparing data from all sites together, a weak  
481 decrease in B/Ca with increasing calcification depth is observed ( $R^2=0.11$ ,  $p < 0.05$ , Fig. S4). A correlation also  
482 exists between B/Ca and the water depths of the cores (not significant, Fig. S4).

483

### 484 5. Discussion

485

#### 486 5.1 Sources of uncertainty relating to depth habitat and seasonality at studied sites

487

##### 488 5.1.1 Depth habitats and $\delta^{11}\text{B}_{\text{borate}}$

489 Because foraminifera will record ambient environmental conditions during calcification, the accurate  
490 characterization of *in situ* data is needed not only for calibrations, but also to understand the reconstructed record  
491 of pH or  $p\text{CO}_2$ . The species we examined are ordered here from shallower to deeper depth habitats: *G. ruber* > *T.*  
492 *sacculifer* (sacc) > *T. sacculifer* (w/o sacc) > *O. universa* > *P. obliquiloculata* > *G. menardii* > *N. dutertrei* > *G.*  
493 *tumida* (this study; Birch et al., 2013; Farmer et al., 2007), although the specific water depth will vary depending  
494 on the physical properties of the water column of the site (Kemle-von Mücke and Oberhänsli, 1999). We note that  
495 calculation of absolute calcification depths can be challenging in some cases as many species often transition to  
496 deeper waters at the end of their life cycle prior to gametogenesis (Steinhardt et al., 2015).

497 We find that assumptions about the specific depth habitat a species of foraminifera is calcifying over, in  
498 a given region, can lead to differences of a few per mil in calculated isotopic compositions of borate (Fig. 3).

499 Hence this can cause a bias in calibrations if calcification depths are assumed instead of being calculated (i.e., with  
500  $\delta^{18}\text{O}$  and/or Mg/Ca). Factors including variations in thermocline depth can impact depth habitats for some taxa.  
501 At the sites we examined, most of the sampled species live in deeper depth habitats in the WEP relative to the  
502 Indian Ocean, which in turn is characterized by deeper depth habitats than in the Arabian Sea. In the tropical  
503 Pacific, *T. sacculifer* is usually found deeper than *G. ruber* except at sites characterized by a shallow thermocline,  
504 in which case both species tend to overlap their habitat (e.g., ODP Site 806 in the WEP which has a deeper  
505 thermocline than at ODP Site 847 in the Eastern Equatorial Pacific; EEP) (Rickaby et al., 2005). The difference in  
506 depth habitats for *T. sacculifer* and *N. dutertrei* between the WEP and EEP can be as much as almost 100 m  
507 (Rickaby et al., 2005).

508

### 509 **5.1.2 Seasonality and *in situ* $\delta^{11}\text{B}_{\text{borate}}$**

510 As discussed by Raitzsch et al. (2018), depending of the study area, foraminiferal fluxes can change  
511 throughout the year. Hydrographic parameters related to carbonate chemistry may change across seasons at a given  
512 water depth. We therefore recalculated the theoretical  $\delta^{11}\text{B}_{\text{borate}}$  using seasonal data for temperature and salinity  
513 and annual values for TA and DIC for each depth at each site. The GLODAP (2013) database does not provide  
514 seasonal TA or DIC values.

515 The low sensitivity of  $\delta^{11}\text{B}_{\text{borate}}$  to temperature and salinity means that calculated  $\delta^{11}\text{B}_{\text{borate}}$  for each water  
516 depth at our sites were not strongly impacted (Fig. S1). Thus, these findings support Raitzsch et al. (2018), who  
517 concluded that calculated  $\delta^{11}\text{B}_{\text{borate}}$  values corrected for seasonality was within error of non-corrected values for  
518 each water depth. As Raitzsch et al. (2018) highlight, seasonality might be more important at high latitude sites  
519 where seasonality is more marked, however, the seasonality of primary production will also be more tightly  
520 constrained due to the seasonal progression of winter light limitation and intense vertical mixing and summer  
521 nutrient limitation.

522 Data for our sites suggests that most  $\delta^{11}\text{B}_{\text{borate}}$  variability we observe does not come from seasonality but  
523 from the assumed water depths for calcification. With the exception of a few specific areas such as the Red Sea  
524 (Henehan et al., 2016, Raitzsch et al., 2018), at most sites examined, seasonal  $\delta^{11}\text{B}_{\text{borate}}$  at a fixed depth does not  
525 vary by more than  $\sim 0.2\%$ . We conclude that seasonality has a relatively minor impact on the carbonate system  
526 parameters at the sites we examined.

527

### 528 **5.2 $\delta^{11}\text{B}$ , microenvironment pH and depth habitats**

529 It is common for planktonic foraminifera to have symbiotic relationships with algae (Gast and Caron,  
530 2001; Shaked and de Vargas, 2006). The family Globigerinidae, including *G. ruber*, *T. sacculifer* and *O. universa*,  
531 commonly have dinoflagellate algal symbionts (Anderson and Be, 1976; Spero, 1987). The families  
532 Pulleniatinidae and Globorotaliidae (e.g. *P. obliquiloculata*, *G. menardii* and *G. tumida*) have chrysophyte algal  
533 symbionts (Gastrich, 1988) and *N. dutertrei* hosts pelagophyte symbionts (Bird et al., 2018). The relationship  
534 between the symbionts and the host is complex. Nevertheless, this symbiotic relationship provides energy  
535 (Hallock, 1981b) and promotes calcification in foraminifera (Duguay, 1983; Erez et al., 1983) by providing  
536 inorganic carbon to the host (Jorgensen et al., 1985).

537 There are several studies indicating that the  $\delta^{11}\text{B}$  signatures in foraminiferal calcite reflect  
538 microenvironment pH (Jorgensen et al., 1985; Rink et al., 1998; Köhler-Rink and Köhl, 2000, Hönisch et al., 2003;

539 Zeebe et al., 2003). Foraminifera with high photosynthetic activity and symbiont density, such as *G. ruber* and *T.*  
540 *sacculifer*, are expected to have a microenvironment pH higher than ambient seawater, and a  $\delta^{11}\text{B}_{\text{carbonate}}$  higher  
541 than expected  $\delta^{11}\text{B}_{\text{borate}}$ , which is the case in our study and in previous studies (Foster et al., 2008, Henehan et al.,  
542 2013, Raitzsch et al., 2018). We also observed in our study that *N. dutertrei*, *G. menardii*, *P. obliquiloculata* and  
543 *G. tumida* record a lower pH than ambient seawater, with  $\delta^{11}\text{B}_{\text{carbonate}}$  lower than expected  $\delta^{11}\text{B}_{\text{borate}}$ , and suggest  
544 the results are consistent with lower photosynthetic activity compared to the mixed-layer dwelling species. These  
545 observations, based on  $\delta^{11}\text{B}_{\text{carbonate}}$  measurements, are in line with direct observations from Takagi et al. (2019)  
546 that show dinoflagellate-bearing foraminifera (*G. ruber*, *T. sacculifer* and *O. universa*) tend to have a higher  
547 symbiont density and photosynthesis activity while *P. obliquiloculata*, *G. menardii* and *N. dutertrei* have lower  
548 symbiont density and *P. obliquiloculata*, *N. dutertrei* have the lowest photosynthetic activity. In the same study,  
549 *P. obliquiloculata* exhibited minimum symbiont densities and levels of photosynthetic activity, which may explain  
550 why *P. obliquiloculata* exhibited the lowest microenvironment pH as recorded by  $\delta^{11}\text{B}$ .

551 Based on the observations of Takagi et al. (2019), we can assume that the low  $\delta^{11}\text{B}$  of *O. universa* and *T.*  
552 *sacculifer* (w/o sacc) from the WEP is explained by low photosynthetic activity. It has been shown for *T. sacculifer*  
553 and *O. universa* that symbiont photosynthesis increases with higher insolation (Jorgensen et al., 1985; Rink et al.,  
554 1998) and the photosynthetic activity is therefore a function of the light level the symbionts received. This is, in a  
555 natural system, dependent on the depth of the species in the water column. For the purpose of this study, we do  
556 not consider turbidity which also influences the light penetration in the water column. In this case,  
557 photosynthetically-active foraminifera living close to the surface should record microenvironment pH (thus  $\delta^{11}\text{B}$ )  
558 that is more sensitive to water depth changes. A deeper habitat reduces solar insolation, and as a consequence, may  
559 lower symbiont photosynthetic activity, possibly reducing pH in the foraminifera's microenvironment. This is  
560 supported by the significant trend observed between  $\Delta^{11}\text{B}$  and the calcification depth for *G. ruber* and *T. sacculifer*  
561 at our sites (Fig. S2), where microenvironment pH decreases with calcification depth. We observe a significant  
562 decrease in  $\delta^{11}\text{B}$  in the WEP for *T. sacculifer* (w/o sacc) compared to the other sites ( $p < 0.05$ ). Additionally, the  
563  $\Delta^{11}\text{B}$  ( $\Delta^{11}\text{B} = \delta^{11}\text{B}_{\text{carbonate}} - \delta^{11}\text{B}_{\text{borate}}$ ) of *G. ruber*, *T. sacculifer* (w/o sacc and sacc) is significantly lower in the  
564 WEP compared to the other sites ( $p < 0.05$ ).

565 *T. sacculifer* has the potential to support more photosynthesis due to its higher symbiont density, and  
566 higher photosynthetic activity compared to other species, which may support higher symbiont/host interactions  
567 (Takagi et al., 2019). These results would be consistent with a greater sensitivity of *T. sacculifer*'s photosynthetic  
568 activity with changes in insolation/water depth. To test if the low  $\delta^{11}\text{B}$  signature of *T. sacculifer* (w/o sacc) in the  
569 WEP is related to a decrease in light at greater water depth, we have independently calculated the calcification  
570 depth of the foraminifera based on various light insolation culture experiments (Jorgensen et al., 1985) and the  
571 microenvironment  $\Delta\text{pH}$  derived from our data (Fig. 7A and B). This exercise showed that the low  $\delta^{11}\text{B}$  of *T.*  
572 *sacculifer* (w/o sacc) from the WEP can be explained by the reduced light environment due to a deeper depth  
573 habitat in the WEP (Fig. 7B). It can also be noted that *T. sacculifer* exhibits the largest variation in symbiont  
574 density versus test size (Takagi et al., 2019), suggesting that lower size fraction reported for the WEP (250-400  
575  $\mu\text{m}$ ) compared to the 300-400  $\mu\text{m}$  at the other sites can be related to a decrease in photosynthetic activity and a  
576 lower  $\delta^{11}\text{B}$ . Unfortunately, no weight per shell data were determined on foraminifera samples to constrain whether  
577 test size was significantly different across sites. Future studies could use shell weights to test these relationships.

578 When the same approach of independently reconstructing calcification depth based on culture  
579 experiments is applied to *O. universa*, the boron data suggest a microenvironment pH of 0.10 to 0.20 lower than  
580 ambient seawater pH, which would be in line with the species living deeper than 50m (light compensation point  
581 (Ec), Rink et al., 1998), which is consistent with our calcification depth reconstructions. The low  $\delta^{11}\text{B}_{\text{carbonate}}$  of  
582 *O. universa* compared to *T. sacculifer* for the similar calcification depth at some sites (e.g. FC-02a, WP07-a) might  
583 reflect differences in photosynthetic potential between the two species, which is supported by observation of a  
584 lower photosynthetic potential in *O. universa* than in *T. sacculifer* (Tagaki et al., 2019).

585 Microenvironment  $\Delta\text{pH}$  based on our  $\delta^{11}\text{B}_{\text{carbonate}}$  data were calculated for the rest of the species. We  
586 observed that microenvironment  $\Delta\text{pH}$  is higher in *T. sacculifer* > *G. ruber* > *T. sacculifer* (w/o sacc - WEP) > *O.*  
587 *universa*, *N. dutertrei*, *G. menardii*, *G. tumida* > *P. obliquiloculata*. These results are in line with the  
588 photosymbiosis findings from Takagi et al., (2019). Also, the higher  $\delta^{11}\text{B}$  data from the West African upwelling  
589 published by Raitzsch et al., (2018) for *G. ruber* and *O. universa* may reflect a higher microenvironment pH due  
590 to a relatively shallow habitat, higher insolation and high rates of photosynthesis by symbionts. This could  
591 highlight a potential issue with calibration when applied to sites with different oceanic regimes as the  $\delta^{11}\text{B}$  species-  
592 specific calibrations could be also location-specific for the mixed dweller species.

593 Microenvironment pH for *N. dutertrei*, *G. menardii* and *G. tumida* are similar to *O. universa* and suggest  
594 a threshold for a respiration-driven  $\delta^{11}\text{B}$  signature. This threshold can be induced by a change of photosynthetic  
595 activity at lower light intensity in deeper water and/or differences in symbiont density and/or by the type of  
596 symbionts at greater depth (non-dinoflagellate symbionts). We also note that *P. obliquiloculata*, which has the  
597 lowest symbiont density and photosynthetic activity (Takagi et al., 2019), has the lowest microenvironment pH  
598 compared to other deeper-dweller species, supporting our hypothesis that respiration can control  
599 microenvironment pH. The deep-dwelling species sensitivity of  $\delta^{11}\text{B}_{\text{carbonate}}$  to  $\delta^{11}\text{B}_{\text{borate}}$  with values close to unity  
600 might also be explained by a relatively stable respiration-driven microenvironments, as the deeper-dweller species  
601 do not experience large changes of insolation (e.g. photosynthesis), thereby making them a more direct recorder  
602 of environmental pH.

603

### 604 **5.3 $\delta^{11}\text{B}$ sensitivity to $\delta^{11}\text{B}_{\text{borate}}$ and relationship with B/Ca signatures**

605 In inorganic calcite,  $\delta^{11}\text{B}_{\text{carbonate}}$  and B/Ca data have shown to be sensitive to precipitation rate with at  
606 higher precipitation rate increasing  $\delta^{11}\text{B}_{\text{carbonate}}$  (Farmer et al., 2019) and B/Ca (Farmer et al., 2019; Gabitov et al.,  
607 2014; Kaczmarek et al., 2016; Mavromatis et al., 2015; Uchikawa et al., 2015). A recent study from Farmer et al,  
608 (2019) has proposed that in foraminifera at higher precipitation rates, more borate ion may be incorporated into  
609 the carbonate mineral, while more boric acid may be incorporated at lower precipitation rates. The authors also  
610 suggest this may explain low sensitivities of culture experiments.

611 When combining all literature data, *T. sacculifer* and *G. ruber* have sensitivities of  $\delta^{11}\text{B}_{\text{carbonate}}$  to  $\delta^{11}\text{B}_{\text{borate}}$   
612 of  $0.83 \pm 0.48$  and  $0.46 \pm 0.34$  respectively in line with previous literature and paleo- $\text{CO}_2$  reconstructions. Also, if  
613 we only take into account our data, and the observation that the sensitivity of  $\delta^{11}\text{B}_{\text{carbonate}}$  to  $\delta^{11}\text{B}_{\text{borate}}$  is not  
614 statistically different from unity for most of the species investigated, we can speculate that for these taxa, changes  
615 in precipitation rate and contributions of boric acid are not likely to be important. If considering only the data from  
616 this study, *G. ruber* ( $1.12 \pm 1.67$ ) and *T. sacculifer* ( $1.38 \pm 1.35$ ) present higher sensitivities of  $\delta^{11}\text{B}_{\text{carbonate}}$  to  
617  $\delta^{11}\text{B}_{\text{borate}}$ . We can then again speculate that the observed high values for  $\delta^{11}\text{B}_{\text{carbonate}}$  at high seawater pH can be due



618 to higher precipitation rates. We note this could also be consistent with the higher sensitivity of B/Ca signatures  
619 in these two surface dwelling species to ambient  $[B(OH)_4^-]/[HCO_3^-]$  relative to deeper-dwelling species. Those  
620 interspecific differences still remain to be explained, however, part of this variability is likely due to changes in  
621 the carbonate chemistry of the microenvironment resulting in changing competition between borate and  
622 bicarbonate. A caveat is that we can not exclude specific biological processes, and that in taxa with a non  
623 respiration-driven microenvironment, changes in day/night calcification ratios also impacting observed values. As  
624 indicated by Farmer et al., (2019), studies of calcite precipitation rates in foraminifera may help to improve our  
625 understanding of the fundamental basis of boron-based proxies.

626

#### 627 **5.4 Evaluation of species for pH reconstructions and water depth pH reconstructions**

628 This data set allows us to reassess the utility of boron-based proxies for the carbonate system. The main  
629 aim of using boron-based proxies relates to the reconstruction of past oceanic conditions, specifically pH and  
630 pCO<sub>2</sub>. Mixed-layer species (eg. *G. ruber* and *T. sacculifer*) are potential archives for atmospheric CO<sub>2</sub>  
631 reconstructions. Other species can shed light on other aspects of the carbon cycle including the physical and  
632 biological carbon pumps.

633 There are a few main inferences we can make. When integrated with published data, the sensitivities of  
634  $\delta^{11}B_{\text{carbonate}}$  to  $\delta^{11}B_{\text{borate}}$  for *G. ruber* and *T. sacculifer* are similar to previous studies (Martinez-Boti et al., 2015b;  
635 Raitzsch et al., 2018) which supports the fidelity of previous paleo-reconstructions that use published calibrations  
636 between  $\delta^{11}B_{\text{carbonate}}$  and  $\delta^{11}B_{\text{borate}}$ . The regression we have made for *G. ruber* supports a decrease in  $\delta^{11}B_{\text{carbonate}}$   
637 with decreasing size fractions (offset of -0.4 ‰, p>0.05) with the sensitivity of  $\delta^{11}B_{\text{carbonate}}$  to  $\delta^{11}B_{\text{borate}}$  not being  
638 statistically different from higher size fraction (p<0.05). The variability in our weight per shell for our *G. ruber*,  
639 based data from Henehan et al. (2013), can potentially imply a deviation down to 1‰ relative to calibration line  
640 from Henehan et al. (2013), which can be in line with the maximum deviation observed in our data (~1.2 ‰) and  
641 not inconsistent with a size effect explaining the offset in our calibration. Our  $\delta^{11}B_{\text{carbonate}}$  data and the sensitivity  
642 to  $\delta^{11}B_{\text{borate}}$  of *O. universa* supports previous data from Henehan et al. (2016). *N. dutertrei*  $\delta^{11}B_{\text{carbonate}}$  data span a  
643 large range of pH, allowing us to derive a robust calibration with  $\delta^{11}B_{\text{borate}}$ . It remains premature to assume that a  
644 unique calibration with a slope of ~-0.9 can be used for all deeper-dwelling species, more data is needed for *P.*  
645 *obliquiloculata*, *G. menardii* and *G. tumida* to robustly test this assertion.

646 In order to derive accurate reconstructions of past ambient pH and pCO<sub>2</sub>, accurate species-specific  
647 calibrations need to be used that are constrained by core-tops or samples from similar types of settings (Fig. 8, 10,  
648 S6). Lower  $\delta^{11}B$  signatures in *T. sacculifer* (w/o sacc) are observed in the WEP, which may be explained by the  
649 deeper depth habitat for this taxa, as lower light levels might reduce symbiont photosynthetic activity. Also, we  
650 show that a correction is needed for *T. sacculifer* (w/o sacc) in the WEP in order to accurately reconstruct  
651 atmospheric CO<sub>2</sub>. When applying calibrations n°2 and 4 to *T. sacculifer* and *G. ruber* (compilation of all data,  
652 Table 3) our data show more variability, especially for *G. ruber* which lead to the larger mismatch compared to *in*  
653 *situ* parameters. The greater divergence of reconstructed values from *in situ* measurements are observed at site  
654 WPO7-01 for both *T. sacculifer* (w/o sacc) and *G. ruber*. More data would be needed to determine a proper  
655 correction for both species and coretop study will be determinant for future downcore reconstructions, especially  
656 in the WEP. We also find that for two species, the boron isotope-pH proxy is a relatively straightforward recorder  
657 of ambient pH, with sensitivities close to unity observed for *O. universa* and *N. dutertrei*.

658           There is also promise in using multiple species in a sample from different hydrographic regimes to  
659 reconstruct vertical profiles of pH and pCO<sub>2</sub>. We are able to reproduce pH and pCO<sub>2</sub> profiles from multiple sites  
660 with different water column structures (Fig. 8) with those reconstructions within error of the *in situ* values, for  
661 most sites. In order to avoid circularity, to validate these calibrations, we recalculated ambient pH and pCO<sub>2</sub> by  
662 first excluding site-specific data and then recalculating species-specific calibrations, followed by application to  
663 each specific site. The comparison of the two methods, first using all the data to derive the calibration and  
664 recalculate pH and pCO<sub>2</sub> (circular) and the second by excluding the site of interest, derive calibrations and calculate  
665 pH and pCO<sub>2</sub> (not circular), does not show significant differences and validates the robustness of the calibrations  
666 (Fig. S5). We utilized the calibrations derived from our data for *G. ruber* (calibration n°1 and 2, Table 3), *T.*  
667 *sacculifer* (calibration n°3 and 4, Table 3), *O. universa* (calibration n°8, Table 3), for *P. obliquiloculata* (calibration  
668 n°11, Table 3), and for *N. dutertrei*, *G. tumida* and *G. menardii* the calibration made on the compilation of the  
669 deep-dweller (calibration n°13, Table 3). Results are shown in Fig. 8 and evaluated in Fig. 9. For *G. menardii*,  
670 more data would be helpful to provide additional constraints. Results for *G. ruber* are the most scattered,  
671 potentially due to difference in test sizes (Henehan et al., 2013), or depth habitat. Results reaffirm the importance  
672 of working with narrow size fractions (Henehan et al., 2013), the utilization of calibrations derived from the same  
673 size fraction or use of offsets to take into account this size fraction effect, and the importance of core-top studies  
674 before paleo-application.

675

## 676 **6. Conclusions and future implications**

677           Our study has extended the boron isotope proxy with data for new species and sites. The work supports  
678 previous work showing that depth habitats of foraminifera vary depending on the oceanic regime, and this can  
679 impact boron isotope signatures. Low δ<sup>11</sup>B values in the WEP compared to other regions for *T. sacculifer* (w/o  
680 sacc) may be explained by a reduction in microenvironment pH due to a deeper depth habitat associated with  
681 reduced irradiance and thus photosynthetic activity.

682           In order to accurately develop downcore reconstructions, constraining the depth habitat using core-tops  
683 studies is important, as a same species can record the seawater pH at different water depth potentially introducing  
684 biases when comparing between different locations. Also, we speculate that a change of the thermocline depth in  
685 the past could imply variations of depth habitat and introduce biases in the reconstructions but further work is  
686 needed to test this assertion.

687           The sensitivity of δ<sup>11</sup>B<sub>carbonate</sub> to pH is in line with previously published data for *T. sacculifer*, *G. ruber*.  
688 The sensitivity of δ<sup>11</sup>B<sub>carbonate</sub> to pH of *O. universa* (mixed-dweller), *N. dutertrei*, *G. menardii* and *G. tumida* (deep-  
689 dwellers) are similar but more data are needed to fully determine those sensitivities. The similarity of boron isotope  
690 calibrations for deep-dwelling taxa might be related to similar respiration-driven microenvironments.

691           Reconstruction of seawater pH and carbonate system parameters is achievable using foraminiferal δ<sup>11</sup>B  
692 but additional core-top and down-core studies reconstructing depth profiles will be needed in order to further verify  
693 calibrations published to date. Past pH and pCO<sub>2</sub> water depth profiles can potentially be created by utilizing  
694 multiple foraminiferal species in concert with taxon-specific calibrations for similar settings. This approach has  
695 much potential for enhancing our understanding of the past workings of the oceanic carbon cycle, and the  
696 biological pump.

697

698 **Author contribution**

699 R.E and A.T. wrote the proposals that funded the work. A.T. and F.C. provided the samples. M.G., S.M. and A.T.  
700 contributed to the experimental design. A.V. helped for sample preparation. M.G. and S.M contributed to  
701 developing the method of boron isotope analysis. M.G. performed the measurements with assistance from S.M.  
702 M.G conducted the data analysis. M.G. drafted the paper, which was edited by all authors. Interpretation was led  
703 by M.G., A.T., S.M. with input from R.E., A.V. and F.C.

704

705 **Competing interests**

706 The authors declare that they have no conflict of interest.

707

708 **Acknowledgments:**

709 The authors wish to thank Jesse Farmer for his valuable and detailed comments on the actual and a previous version  
710 of the manuscript. We wish to thank Michael Henehan for helpful discussion, comments on the manuscript and  
711 help with the code. We also want to thank the anonymous reviewer for helpful comments. Lea Bonnin for  
712 assistance with picking samples, the IODP repository for provision of samples, the Tripati Laboratory (UCLA) for  
713 their technical support, Mervyn Greaves, Madeleine Bohlin (University of Cambridge) for technical support and  
714 use of laboratory space, Yoan Germain, Emmanuel Ponzevera and Oanez Lebeau for technical support and use of  
715 laboratory space in Brest, Jill Sutton for helpful conversation on the manuscript. Research is supported by DOE  
716 BES grant DE-FG02-13ER16402, by the International Research Chair Program that is funded by the French  
717 government (LabexMer ANR-10-LABX-19-01), and IAGC student research grant 2017.

718

719 **References**

- 720 Allen, K. A. and Hönisch, B.: The planktic foraminiferal B/Ca proxy for seawater carbonate chemistry, A critical  
721 evaluation, *Earth Planet. Sci. Lett.*, 345–348, 203–211, 2012.
- 722 Anagnostou, E., John, E., Edgar, K., Foster, G., Ridgwell, A., Inglis, G., Pancost, R., Lunt, D. and Pearson, P.,  
723 Changing atmospheric CO<sub>2</sub> concentration was the primary driver of early Cenozoic climate: *Nature* 533,  
724 380–384, 2016.
- 725 Anand, P., Elderfield, H. and Conte, M. H., Calibration of Mg/Ca thermometry in planktonic foraminifera from a  
726 sediment trap time series. *Paleoceanography* 18, 2003.
- 727 Anderson, O. R. and Bé, A.W. H.: The ultrastructure of a planktonic foraminifer, *Globigerinoides sacculifer*  
728 (Brady), and its symbiotic dinoflagellates: *J. Foramin. Res.*, 6, 1–21, 1976.
- 729 Axelsson, M. D., Rodushkin, I., Ingri, J. and Öhlander, B.: Multielemental analysis of Mn–Fe nodules by ICP-  
730 MS: optimisation of analytical method, *Analyst*, 127, 76–82, 2002.
- 731 Babila, T.L., Rosenthal, Y., Conte, M.H.: Evaluation of the biogeochemical controls on B/Ca of *Globigerinoides*  
732 *ruber* white from the Oceanic Flux Pro-gram, Bermuda, *Earth Planet. Sci. Lett.* 404, 67–76, 2014.
- 733 Barker, S., Greaves M. and Elderfield, H.: A study of cleaning procedures used for foraminiferal Mg/Ca  
734 paleothermometry, *Geochemistry, Geophys. Geosystems* 4, 1–20, 2003.
- 735 Bartoli, G., Hönisch, B. and Zeebe, R. E.: Atmospheric CO<sub>2</sub> decline during the Pliocene intensification of  
736 Northern Hemisphere glaciations, *Paleoceanography* 26, 1–14, 2011.
- 737 Bemis, B. E., Spero, H. J., Bijma, J. and Lea, D. W.: Reevaluation of the oxygen isotopic composition of  
738 planktonic foraminifera: Experimental results and revised paleotemperature equations, *Paleoceanography*  
739 13, 150–160, 1998.
- 740 Bemis, B. E., Spero, H. J. and Thunell, R. C.: Using species-specific paleotemperature equations with  
741 foraminifera: a case study in the Southern California Bight, *Mar. Micropaleontol.*, 46, 405–430, 2002.
- 742 Bijma, J., Faber Jr., W.W., Hemleben, C.: Temperature and salinity limits for growth and survival of some  
743 planktonic foraminifera in laboratory cultures, *J. Foraminiferal Res.* 20 (2), 95–116, 1990.
- 744 Bijma, J., Hönisch, B. and Zeebe, R. E.: Impact of the ocean carbonate chemistry on living foraminiferal shell  
745 weight: Comment on “Carbonate ion concentration in glacial-age deep waters of the Caribbean Sea” by W.  
746 S. Broecker and E. Clark, *Geochemistry, Geophys. Geosystems*, 3, 1–7, 2002.
- 747 Birch, H., Coxall, H. K., Pearson, P. N., Kroon, D. and O’Regan, M.: Planktonic foraminifera stable isotopes and  
748 water column structure, Disentangling ecological signals, *Mar. Micropaleontol.*, 101, 127–145, 2013.
- 749 Bird, C., Darling, K. F., Russell, A. D., Fehrenbacher, J. S., Davis, C. V., Free, A., & Ngwenya, B. T.: 16S  
750 rRNA gene metabarcoding and TEM reveals different ecological strategies within the genus  
751 *Neogloboquadrina* (planktonic foraminifer), *PloS one*, 13(1), 2018.
- 752 Boyer, T.P., Antonov, J. I., Baranova, O. K., Coleman, C., Garcia, H. E., Grodsky, A., Johnson, D. R., Locarnini,  
753 R. A., Mishonov, A. V., O’Brien, T.D., Paver, C.R., Reagan, J.R., Seidov, D., Smolyar, I. V., and Zweng,  
754 M. M.: *World Ocean Database*, NOAA Atlas NESDIS 72, S. Levitus, Ed., A. Mishonov, Technical Ed.,  
755 Silver Spring, MD, 209, 2013.
- 756 Boyle, E. A., Cadmium, zinc, copper, and barium in foraminifera tests, *Earth Planet. Sci. Lett.*, 53, 11–35, 1981.

- 757 Boyle, E. A., and L. D., Keigwin, Comparison of Atlantic and Pacific paleochemical records for the Last  
758 215,000 years: Changes in deep ocean circulation and chemical inventories, *Earth Planet. Sci. Lett.*, 76,  
759 135–150, 1985.
- 760 Branson, O., Kaczmarek, K., Redfern, S. A. T., Misra, S., Langer, G., Tyliszczak, T., Bijma, J. and Elderfield,  
761 H., The coordination and distribution of B in foraminiferal calcite, *Earth Planet. Sci. Lett.*, 416, 67–72,  
762 2015.
- 763 Catanzaro, E.J., Champion, C.E., Garner, A.L., Marinenko, G., Sappenfield, K.M. and Shields, W.R.: Boric  
764 Acid; Isotopic and Assay Standard Reference Materials, U.S. Natl. Bur. Stand. Spec., Publ. 260-17, 70p,  
765 1970.
- 766 Chalk, T. B., Hain, M. P., Foster, G. L., Rohling, E. J., Sexton, P. F., Badger, M. P. S., Cherry, S. G., Hasenfratz,  
767 A. P., Haug, G. H., Jaccard, S. L., Martínez-García, A., Pälike, H., Pancost, R. D. and Wilson, P. A.,  
768 Causes of ice age intensification across the Mid-Pleistocene Transition, *Proc. Natl. Acad. Sci.*, 114,  
769 13114–13119, 2017.
- 770 Coadic, R., Bassinot, F., Dissard, D., Douville, E., Greaves, M. and Michel, E., A core-top study of dissolution  
771 effect on B/Ca in Globigerinoides sacculifer from the tropical Atlantic: Potential bias for paleo-  
772 reconstruction of seawater carbonate chemistry, *Geochemistry, Geophys. Geosystems* 14, 1053–1068,  
773 2013.
- 774 de Nooijer, L. J., Spero, H. J., Erez, J., Bijma, J. and Reichart, G. J., Biomineralization in perforate foraminifera.  
775 *Earth-Science Rev.*, 135, 48–58, 2014.
- 776 Dekens, P. S., Lea, D. W., Pak, D. K. and Spero, H. J., Core top calibration of Mg/Ca in tropical foraminifera,  
777 Refining paleotemperature estimation, *Geochemistry, Geophys. Geosystems* 3, 1–29, 2002.
- 778 Deuser, W.G., Ross, E.H., Hemleben, Ch., Spindler, M., Seasonal changes in species composition, numbers,  
779 mass, size, and isotopic composition of planktonic foraminifera settling into the deep Sargasso Sea,  
780 *Palaeogeogr., Palaeoclimat., Palaeoecol.*, 33:103-127, 1981.
- 781 Deuser, W. G. and Ross, E. H., Seasonally abundant planktonic foraminifera of the Sargasso Sea; succession,  
782 deep-water fluxes, isotopic compositions, and paleoceanographic implications, *J. Foraminifer. Res.* 19,  
783 268–293, 1989.
- 784 Dickson, A. G., Thermodynamics of the dissociation of boric acid in synthetic seawater from 273.15 to 318.15  
785 K., *Deep Sea Res., Part A, Oceanogr. Res. Pap.* 37, 755–766, 1990.
- 786 Dickson, A.G., Millero, F.J., A comparison of the equilibrium constants for the dissociation of carbonic acid in  
787 seawater media, *Deep-Sea Res.*, 34, 1733–1743, 1987.
- 788 Douville, E., Paterne, M., Cabioch, G., Louvat, P., Gaillardet, J., Juillet-Leclerc, A. and Ayliffe, L., Abrupt sea  
789 surface pH change at the end of the Younger Dryas in the central sub-equatorial Pacific inferred from  
790 boron isotope abundance in corals (*Porites*), *Biogeosciences* 7, 2445–2459, 2010.
- 791 Duguay, L.E., Comparative laboratory and field studies on calcification and carbon fixation in foraminiferal-  
792 algal associations, *Journal of Foraminiferal Research* 13, 252-261, 1983.
- 793 Duplessy, J., Labeyrie, L., Juilletleclerc, A., Maitre, F., Duprat, J. and Sarnthein, M.: Surface salinity  
794 reconstruction of the north-atlantic ocean during the last glacial maximum, *Oceanol. Acta*, 14, 311–324,  
795 1991.
- 796 Elderfield, H., Yu, J., Anand, P., Kiefer, T. and Nyland, B., Calibrations for benthic foraminiferal Mg/Ca  
797 paleothermometry and the carbonate ion hypothesis, *Earth Planet. Sci. Lett.*, 250, 633–649., 2006.

- 798 Elderfield, H. and Granssen, G., Past temperatures and O18 of surface ocean waters inferred from foraminiferal  
799 Mg/Ca ratios, *Nature* 405, 442–445, 2000.
- 800 Erez J., Calcification Rates, Photosynthesis and Light in Planktonic Foraminifera. In: Westbroek P., de Jong  
801 E.W. (eds) *Biom mineralization and Biological Metal Accumulation*. Springer, Dordrecht, 1983.
- 802 Erez, J., The Source of Ions for Biom mineralization in Foraminifera and Their Implications for Paleoceanographic  
803 Proxies, *Rev. Mineral. Geochemistry*, 54, 115–149, 2003.
- 804 Fairbanks, R. G. and Wiebe, P. H.: Foraminifera and Chlorophyll Maximum: Vertical Distribution, Seasonal  
805 Succession, and Paleoceanographic Significance, *Science*, 209, 1524–1526, 1980.
- 806 Fairbanks, R. G., Sverdløve, M., Free, R., Wiebe, P. H. and Bé, A. W. H.: Vertical distribution and isotopic  
807 fractionation of living planktonic foraminifera from the Panama Basin, *Nature*, 298, 841–844, 1982.
- 808 Farmer, E. C., Kaplan, A., de Menocal, P. B. and Lynch-Stieglitz, J., Corroborating ecological depth preferences  
809 of planktonic foraminifera in the tropical Atlantic with the stable oxygen isotope ratios of core top  
810 specimens, *Paleoceanography*, 22, 1–14, 2007.
- 811 Farmer, J. R., Hönisch, B., & Uchikawa, J.: Single laboratory comparison of MC-ICP-MS and N-TIMS boron  
812 isotope analyses in marine carbonates, *Chemical Geology*, 447, 173–182, 2016.
- 813 Farmer, J. R., Branson, O., Uchikawa, J., Penman, D. E., Hönisch, B., & Zeebe, R. E.: Boric acid and borate  
814 incorporation in inorganic calcite inferred from B/Ca, boron isotopes and surface kinetic modeling,  
815 *Geochimica et Cosmochimica Acta*, 244, 229–247, 2019.
- 816 Feely, R., Impact of Anthropogenic CO<sub>2</sub> on the CaCO<sub>3</sub> System in the Oceans, *Science*, 305, 362–366, 2004.
- 817 Ferguson, J. E., Henderson, G. M., Kucera, M. and Rickaby, R. E. M.: Systematic change of foraminiferal  
818 Mg/Ca ratios across a strong salinity gradient, *Earth Planet. Sci. Lett.*, 265, 153–166, 2008.
- 819 Foster, G. L., Seawater pH, pCO<sub>2</sub> and [CO<sub>3</sub><sup>2-</sup>] variations in the Caribbean Sea over the last 130 kyr: A boron  
820 isotope and B/Ca study of planktic foraminifera, *Earth Planet. Sci. Lett.*, 271, 254–266, 2008.
- 821 Foster, G. L. and Sexton, P. F.: Enhanced carbon dioxide outgassing from the eastern equatorial Atlantic during  
822 the last glacial, *Geology*, 42, 1003–1006, 2014.
- 823 Foster, G. L., Lear, C. H. and Rae, J. W. B., The evolution of pCO<sub>2</sub>, ice volume and climate during the middle  
824 Miocene, *Earth Planet. Sci. Lett.*, 341–344, 243–254, 2012.
- 825 Foster, G. L. and Rae, J. W. B., Reconstructing Ocean pH with Boron Isotopes in Foraminifera, *Annu. Rev.*  
826 *Earth Planet. Sci.*, 44, 207–237, 2016.
- 827 Gabitov, R. I., Rollion-bard, C., Tripathi, A. and Sadekov, A., In situ study of boron partitioning between calcite  
828 and fluid at different crystal growth rates, *Geochim. Cosmochim. Acta*, 137, 81–92, 2014.
- 829 Gaillardet, J., Lemarchand, D., Göpel, C. and Manhès, G., Evaporation and Sublimation of Boric Acid :  
830 Application for Boron Purification from Organic Rich Solutions, *Geostand. Newsl.*, 25, 67–75, 2001.
- 831 Gast, R. J. and Caron D. A., Photosymbiotic associations in planktonic foraminifera and radiolaria, 1–7, 2001.
- 832 Gastrich, M.D., Ultrastructure of a new intracellular symbiotic alga found within planktonic foraminifera,  
833 *Journal of Phycology* 23, 623–632, 1988.
- 834 Gattuso, J.P. and Hansson, L., *Ocean acidification*, Oxford University Press, 2011.

- 835 Gutjahr, M., Bordier, L., Douville, E., Farmer, J., Foster, G. L., Hathorne, E., Hönisch, B., Lemarchand, D., Louvat,  
836 P., McCulloch, M., Noireaux, J., Pallavicini, N., Rodushkin, I., Roux, P., Stewart, J., Thil, F. You, C.F.,  
837 Boron Isotope Intercomparison Project (BIIP): Development of a new carbonate standard for stable isotopic  
838 analyses. In EGU general assembly conference abstracts, Vol. 16, (2014).
- 839 Hallock P., Algal Symbiosis : A Mathematical Analysis Marine Biology 62, 249-255, 1981b.
- 840 Hemming, N. G. and Hanson, G. N. Boron isotopic composition and concentration in modern marine carbonates,  
841 Geochim. Cosmochim. Acta, 56, 537–543, 1992.
- 842 Hendry, K.R., Rickaby, R.E.M., Meredith, M.P., Elderfield, H., Controls on stable isotope and trace metal  
843 uptake in *Neogloboquadrina pachyderma* (sinistral) from an Antarctic sea-ice environment. Earth Planet.  
844 Sci. Lett. 278, 67–77, 2009.
- 845 Henehan, M. J., Foster, G. L., Bostock, H. C., Greenop, R., Marshall, B. J. and Wilson, P. A., A new boron  
846 isotope-pH calibration for *Orbulina universa*, with implications for understanding and accounting for ‘vital  
847 effects’, Earth Planet. Sci. Lett., 454, 282–292, 2016.
- 848 Henehan, M. J., Foster, G. L., Rae, J. W. B., Prentice, K. C., Erez, J., Bostock, H. C., Marshall, B. J. and Wilson,  
849 P. A., Evaluating the utility of B/Ca ratios in planktic foraminifera as a proxy for the carbonate system: A  
850 case study of *Globigerinoides ruber*, Geochemistry, Geophys. Geosystems 16, 1052–1069, 2015.
- 851 Henehan, M. J., Rae, J. W. B., Foster, G. L., Erez, J., Prentice, K. C., Kucera, M., Bostock, H. C., Martínez-Botí,  
852 M. A., Milton, J. A., Wilson, P. A., Marshall, B. J. and Elliott, T., Calibration of the boron isotope proxy in  
853 the planktonic foraminifera *Globigerinoides ruber* for use in palaeo-CO<sub>2</sub> reconstruction, Earth Planet. Sci.  
854 Lett. 364, 111–122, 2013.
- 855 Holcomb, M., Decarlo, T. M., Schoepf, V., Dissard, D., Tanaka, K. and McCulloch, M.: Cleaning and pre-  
856 treatment procedures for biogenic and synthetic calcium carbonate powders for determination of elemental  
857 and boron isotopic compositions, Chem. Geol., 398, 11–21, 2015.
- 858 Hönisch, B., Hemming, N. G., Archer, D., Siddall, M. and McManus, J. F., Atmospheric Carbon Dioxide  
859 Concentration Across the Mid-Pleistocene Transition, Science, 324, 1551–1554, 2009.
- 860 Hönisch, B., Bijma, J., Russell, A. D., Spero, H. J., Palmer, M. R., Zeebe, R. E. and Eisenhauer, A., The  
861 influence of symbiotic photosynthesis on the boron isotopic composition of foraminifera shells, Mar.  
862 Micropaleontol., 49, 87–96, 2003.
- 863 Hönisch, B. and Hemming, N. G., Ground-truthing the boron isotope-paleo-pH proxy in planktonic foraminifera  
864 shells: Partial dissolution and shell size effects, Paleoceanography 19, 1–13, 2004.
- 865 Hönisch, B., Bickert, T. and Hemming, N. G., Modern and Pleistocene boron isotope composition of the benthic  
866 foraminifer *Cibicides wuellerstorfi*, Earth Planet. Sci. Lett., 272, 309–318, 2008.
- 867 Howes, E. L., Kaczmarek, K., Raitzsch, M., Mewes, A., Bijma, N., Horn, I., Misra, S., Gattuso, J. P. and Bijma,  
868 J., Decoupled carbonate chemistry controls on the incorporation of boron into *Orbulina universa*,  
869 Biogeosciences, 14, 415–430, 2017.
- 870 IPCC: Climate Change 2014 - The Physical Science Basis, edited by Intergovernmental Panel on Climate  
871 Change, Cambridge University Press, Cambridge., 2014.
- 872 Jørgensen, B. B., Erez, J., Revsbech, P. and Cohen, Y., Symbiotic photosynthesis in a planktonic foraminifera,  
873 *Globigerinoides sacculifer* (Brady), studied with microelectrodes, Limnol. Oceanogr., 30, 1253–1267  
874 1985.

- 875 Kaczmarek, K., Nehrke, G., Misra, S., Bijma, J. and Elderfield, H., Investigating the effects of growth rate and  
876 temperature on the B/Ca ratio and  $\delta^{11}\text{B}$  during inorganic calcite formation, *Chem. Geol.*, 421, 81–92,  
877 2016.
- 878 Kemle-von Mücke S. and Oberhänsli H., The Distribution of Living Planktic Foraminifera in Relation to  
879 Southeast Atlantic Oceanography, *Use Proxies Paleocenoogr.*, 91–115, 1999.
- 880 Key, R.M., A global ocean carbon climatology: Results from Global Data Analysis Project (GLODAP), *Global*  
881 *Biogeochem. Cycles*, 18, GB4031, 2004.
- 882 Kim, S.T. and O’Neil, J. R., Equilibrium and nonequilibrium oxygen isotope effects in synthetic carbonates,  
883 *Geochim. Cosmochim. Acta*, 61, 3461–3475, 1997.
- 884 Klochko, K., Cody, G. D., Tossell, J. A., Dera, P. and Kaufman, A. J., Re-evaluating boron speciation in  
885 biogenic calcite and aragonite using  $^{11}\text{B}$  MAS NMR, *Geochim. Cosmochim. Acta*, 73, 1890–1900, 2009.
- 886 Klochko, K., Kaufman, A. J., Yao, W., Byrne, R. H. and Tossell, J. A., Experimental measurement of boron  
887 isotope fractionation in seawater, *Earth Planet. Sci. Lett.*, 248, 276–285, 2006.
- 888 Köhler-Rink, S. and Kühl, M., Microsensor studies of photosynthesis and respiration in larger symbiotic  
889 foraminifera. I. The physico-chemical microenvironment of *Marginopora vertebralis*, *Amphistegina*  
890 *lobifera* and *Amphisorus hemrichii*, *Mar. Biol.*, 137, 473–486, 2000.
- 891 Köhler-Rink, S. and Kühl, M., Microsensor studies of photosynthesis and respiration in the larger symbiont  
892 bearing foraminifera *Amphistegina lobifera*, and *Amphisorus hemprichii*, *Ophelia*, 55, 111–122, 2001.
- 893 Lea, D. W., Pak, D. K. and Spero, H. J., Climate impact of late quaternary equatorial Pacific sea surface  
894 temperature variations, *Science*, 289, 1719–1724, 2000.
- 895 Lemarchand, D., Gaillardet, J., Lewin, A. and Allègre, C. J., Boron isotope systematics in large rivers:  
896 Implications for the marine boron budget and paleo-pH reconstruction over the Cenozoic, *Chem. Geol.*,  
897 190, 123–14, 2002.
- 898 Liu, Y., Liu, W., Peng, Z., Xiao, Y., Wei, G., Sun, W., He, J., Liu, G. and Chou, C.L., Instability of seawater pH  
899 in the South China Sea during the mid-late Holocene: Evidence from boron isotopic composition of corals,  
900 *Geochim. Cosmochim. Acta*, 73, 1264–1272, 2009.
- 901 Lloyd, N. S., Sadekov, A. Y. and Misra, S., Application of 1013ohm Faraday cup current amplifiers for boron  
902 isotopic analyses by solution mode and laser ablation multicollector inductively coupled plasma mass  
903 spectrometry, *Rapid Commun. Mass Spectrom.*, 32, 9–18, 2018.
- 904 Martínez-Botí, M. A., Foster, G. L., Chalk, T. B., Rohling, E. J., Sexton, P. F., Lunt, D. J., Pancost, R. D.,  
905 Badger, M. P. S. and Schmidt, D. N., Plio-Pleistocene climate sensitivity evaluated using high-resolution  
906 CO<sub>2</sub> records, *Nature*, 518, 49–54, 2015a.
- 907 Martínez-Botí M. A., Marino G., Foster G. L., Ziveri P., Henahan M. J., Rae J. W. B., Mortyn P. G. and Vance  
908 D., Boron isotope evidence for oceanic carbon dioxide leakage during the last deglaciation. *Nature*, 518,  
909 219–222, 2015b.
- 910 Martínez-Botí, M. A., Mortyn, P. G., Schmidt, D. N., Vance, D. and Field, D. B., Mg/Ca in foraminifera from  
911 plankton tows: Evaluation of proxy controls and comparison with core tops, *Earth Planet. Sci. Lett.*, 307,  
912 113–125, 2011.
- 913 Mavromatis, V., Montouillout, V., Noireaux, J., Gaillardet, J. and Schott, J., Characterization of boron  
914 incorporation and speciation in calcite and aragonite from co-precipitation experiments under controlled  
915 pH, temperature and precipitation rate, *Geochim. Cosmochim. Acta*, 150, 299–313, 2015.



- 916 McCulloch, M. T., D'Olivo, J. P., Falter, J. L., Georgiou, L., Holcomb, M., Montagna, P. and Trotter, J. A.,  
 917 Boron Isotopic Systematics in Scleractinian Corals and the Role of pH Up-regulation, *Boron Isot. Adv.*  
 918 *Isot. Geochemistry*, 2018.
- 919 Misra, S., Greaves, M., Owen, R., Kerr, J., Elmore, A. C. and Elderfield, H.: Determination of B/Ca of natural  
 920 carbonates by HR-ICP-MS, *Geochemistry, Geophys. Geosystems*, 15, 1617–1628, 2014a.
- 921 Misra, S., Owen, R., Kerr, J., Greaves, M. and Elderfield, H., Determination of  $\delta^{11}\text{B}$  by HR-ICP-MS from mass  
 922 limited samples: Application to natural carbonates and water samples, *Geochim. Cosmochim. Acta*, 140,  
 923 531–552, 2014b.
- 924 Mortyn, P. G. and Charles, C. D., Planktonic foraminiferal depth habitat and  $\delta^{18}\text{O}$  calibrations: Plankton tow  
 925 results from the Atlantic sector of the Southern Ocean, *Paleoceanography*, 18, 2003.
- 926 Mulitza, S., Boltovskoy, D., Donner, B., Meggers, H., Paul, A. and Wefer, G., Temperature: $\delta^{18}\text{O}$  relationships  
 927 of planktonic foraminifera collected from surface waters, *Palaeogeogr. Palaeoclimatol. Palaeoecol.*, 202,  
 928 143–152, 2003.
- 929 Ni, Y., Foster, G. L., Bailey, T., Elliott, T., Schmidt, D. N., Pearson, P., Haley, B. and Coath, C., A core top  
 930 assessment of proxies for the ocean carbonate system in surface-dwelling foraminifers, *Paleoceanography*  
 931 22, 2007.
- 932 Nir, O., Vengosh, A., Harkness, J. S., Dwyer, G. S. and Lahav, O., Direct measurement of the boron isotope  
 933 fractionation factor: Reducing the uncertainty in reconstructing ocean paleo-pH, *Earth Planet. Sci. Lett.*,  
 934 414, 1–5, 2015.
- 935 Noireaux, J., Mavromatis, V., Gaillardet, J., Schott, J., Montouillout, V., Louvat, P., Rollion-Bard, C. and  
 936 Neuville, D. R., Crystallographic control on the boron isotope paleo-pH proxy, *Earth Planet. Sci. Lett.*,  
 937 430, 398–407, 2015.
- 938 Orr, J. C., Fabry, V. J., Aumont, O., Bopp, L., Doney, S. C., Feely, R. A., Gnanadesikan, A., Gruber, N., Ishida,  
 939 A., Joos, F., Key, R. M., Lindsay, K., Maier-Reimer, E., Matear, R., Monfray, P., Mouchet, A., Najjar, R.  
 940 G., Plattner, G. K., Rodgers, K. B., Sabine, C. L., Sarmiento, J. L., Schlitzer, R., Slater, R. D., Totterdell, I.  
 941 J., Weirig, M. F., Yamanaka, Y. and Yool, A., Anthropogenic ocean acidification over the twenty-first  
 942 century and its impact on calcifying organisms, *Nature*, 437, 681–686, 2005.
- 943 Pagani, M., Marked Decline in Atmospheric Carbon Dioxide Concentrations During the Paleogene, *Science*,  
 944 309, 600–603, 2005.
- 945 Palmer, M. R., Pearson, P. N. and Cobb, S. J., Reconstructing Past Ocean pH-Depth Profiles, *Science*, 282,  
 946 1468–1471, 1998.
- 947 Pearson, P. N. and Palmer, M. R., Middle Eocene seawater pH and atmospheric carbon dioxide concentrations,  
 948 *Science*, 284, 1824–1826, 1999.
- 949 Peeters, F. J. C. and Brummer, G.J. a., The seasonal and vertical distribution of living planktic foraminifera in  
 950 the NW Arabian Sea, *Geol. Soc. London, Spec. Publ.*, 195, 463–497, 2002.
- 951 Quintana Krupinski, N. B., Russell, A. D., Pak, D. K. and Paytan, A., Core-top calibration of B/Ca in Pacific  
 952 Ocean *Neogloboquadrina incompta* and *Globigerina bulloides* as a surface water carbonate system proxy,  
 953 *Earth Planet. Sci. Lett.*, 466, 139–151, 2017.
- 954 Rae, J.W.B.: Boron Isotopes in Foraminifera: Systematics, Biomineralisation, and CO<sub>2</sub> Reconstruction. In,  
 955 Marschall, H., Foster, G. (eds), *Boron Isotopes. Advances in Isotope Geochemistry*. Springer, Cham, 2018.
- 956 Rae, J. W. B., Foster, G. L., Schmidt, D. N. and Elliott, T., Boron isotopes and B/Ca in benthic foraminifera:  
 957 Proxies for the deep ocean carbonate system, *Earth Planet. Sci. Lett.*, 302, 403–413, 2011.

- 958 Raitzsch, M., Bijma, J., Benthien, A., Richter, K.-U., Steinhofel, G. and Kučera, M., Boron isotope-based  
959 seasonal paleo-pH reconstruction for the Southeast Atlantic – A multispecies approach using habitat  
960 preference of planktonic foraminifera, *Earth Planet. Sci. Lett.*, 487, 138–150, 2018.
- 961 Ravelo, A. C. and Fairbanks, R. G., Oxygen isotopic composition of multiple species of planktonic foraminifera:  
962 recorder of the modern photic zone temperature gradient, *Palaeogeogr. Palaeoclimatol. Palaeoecol.*, 7,  
963 815–831, 1992.
- 964 Rebotim, A., Voelker, A. H. L., Jonkers, L., Waniek, J. J., Meggers, H., Schiebel, R., Fraile, I., Schulz, M., and  
965 Kucera, M., Factors controlling the depth habitat of planktonic foraminifera in the subtropical eastern  
966 North Atlantic, *Biogeosciences*, 14, 827–859, <https://doi.org/10.5194/bg-14-827-2017>, 2017.
- 967 Regenberg, M., Steph, S., Nürnberg, D., Tiedemann, R. and Garbe-Schönberg, D.: Calibrating Mg/Ca ratios of  
968 multiple planktonic foraminiferal species with  $\delta^{18}\text{O}$ -calcification temperatures, *Paleothermometry for the*  
969 *upper water column*, *Earth Planet. Sci. Lett.*, 278, 324–336, 2009.
- 970 Rickaby, R. E. M. and Halloran, P., Cool La Nina During the Warmth of the Pliocene?, *Science*, 307, 1948–  
971 1952, 2005.
- 972 Ries, J. B., Cohen, A. L. and McCorkle, D. C., Marine calcifiers exhibit mixed responses to CO<sub>2</sub>-induced ocean  
973 acidification, *Geology*, 37, 1131–1134, 2009.
- 974 Rink, S., Kühl, M., Bijma, J. and Spero, H. J., Microsensor studies of photosynthesis and respiration in the  
975 symbiotic foraminifer *Orbulina universa*, *Mar. Biol.*, 131, 583–595, 1998.
- 976 Rollion-Bard, C. and Erez, J., Intra-shell boron isotope ratios in the symbiont-bearing benthic foraminiferan  
977 *Amphistegina lobifera*: Implications for  $\delta^{11}\text{B}$  vital effects and paleo-pH reconstructions, *Geochim.*  
978 *Cosmochim. Acta*, 74, 1530–1536, 2010.
- 979 Rostek, F., Ruhland, G., Bassinot, F. C., Muller, P. J., Labeyrie, L. D., Lancelot, Y. and Bard, E., Reconstructing  
980 Sea-Surface Temperature and Salinity Using  $\delta^{18}\text{O}$  and Alkenone Records, *Nature*, 364, 319–321, 1993.
- 981 Russell, A. D., Hönisch, B., Spero, H. J. and Lea, D. W., Effects of seawater carbonate ion concentration and  
982 temperature on shell U, Mg, and Sr in cultured planktonic foraminifera, *Geochim. Cosmochim. Acta*, 68,  
983 4347–4361, 2004.
- 984 Sanyal, A., Bijma, J., Spero, H. J. and Lea, D. W., Empirical relationship between pH and the boron isotopic  
985 composition of *Globigerinoides sacculifer*: Implications for the boron isotopes paleo-pH proxy,  
986 *Paleoceanography*, 16, 515–519, 2001.
- 987 Sanyal, A., Hemming, N. G., Broecker, W. S., Lea, D. W., Spero, H. J., & Hanson, G. N. Oceanic pH control on  
988 the boron isotopic composition of foraminifera: evidence from culture experiments, *Paleoceanography*,  
989 11(5), 513-517, 1996.
- 990 Shaked, Y. and de Vargas, C., Pelagic photosymbiosis: rDNA assessment of diversity and evolution of  
991 dinoflagellate symbionts and planktonic foraminiferal hosts, *Marine Ecology Progress Serie*, 325, 59–71,  
992 2006.
- 993 Schmidt, G. A. and Mulitza, S., Global calibration of ecological models for planktic foraminifera from core-top  
994 carbonate oxygen-18, *Mar. Micropaleontol.*, 44, 125–140, 2002.
- 995 Seki, O., Foster, G. L., Schmidt, D. N., Mackensen, A., Kawamura, K. and Pancost, R. D., Alkenone and boron-  
996 based Pliocene pCO<sub>2</sub> records, *Earth Planet. Sci. Lett.*, 292, 201–211, 2010.
- 997 Shirayama, Y., Effect of increased atmospheric CO<sub>2</sub> on shallow water marine benthos, *J. Geophys. Res.*, 110,  
998 C09S08, 2005.

- 999 Sime, N. G., De La Rocha, C. L. and Galy, A., Negligible temperature dependence of calcium isotope  
1000 fractionation in 12 species of planktonic foraminifera, *Earth Planet. Sci. Lett.*, 232, 51–66, 2005.
- 1001 Spero H. J., Symbiosis in the planktonic foraminifer, *Orbulina universa*, and the isolation of its symbiotic  
1002 dinoflagellate, *gymnodinium beii* sp.nov, *J. Phycol.* 23, 307-317, 1987.
- 1003 Sutton, J. N., Liu, Y. W., Ries, J. B., Guillermic, M., Ponzevera, E. and Eagle, R. A.,  $\delta^{11}\text{B}$  as monitor of  
1004 calcification site pH in divergent marine calcifying organisms, *Biogeosciences*, 15, 1447–1467, 2018.
- 1005 Takagi H., Kimoto K., Fujiki T., Saito H., Schmidt C. and Kucera M., Characterizing photosymbiosis in modern  
1006 planktonic foraminifera, *biogeosciences*, 3377–3396, 2019.
- 1007 Thomson, J., Brown, L., Nixon, S., Cook, G. T. and MacKenzie, A. B., Bioturbation and Holocene sediment  
1008 accumulation fluxes in the north-east Atlantic Ocean (Benthic Boundary Layer experiment sites), *Mar.*  
1009 *Geol.*, 169, 21–39, 2000.
- 1010 Tripathi, A., Deep-Sea Temperature and Circulation Changes at the Paleocene-Eocene Thermal Maximum.  
1011 *Science*, 308, 1894–1898, 2005.
- 1012 Tripathi, A. K., Roberts, C. D. and Eagle, R. A., Coupling of CO<sub>2</sub> and Ice Sheet Stability Over Major Climate  
1013 Transitions of the Last 20 Million Years, *Science*, 326, 1394–1397, 2009.
- 1014 Tripathi, A. K., Roberts, C. D., Eagle, R. A. and Li, G., A 20 million year record of planktic foraminiferal B/Ca  
1015 ratios: Systematics and uncertainties in pCO<sub>2</sub> reconstructions, *Geochim. Cosmochim. Acta*, 75, 2582–  
1016 2610, 2011.
- 1017 Uchikawa, J., Penman, D. E., Zachos, J. C. and Zeebe, R. E., Experimental evidence for kinetic effects on B/Ca  
1018 in synthetic calcite: Implications for potential B(OH)<sub>4</sub><sup>-</sup> and B(OH)<sub>3</sub> incorporation, *Geochim. Cosmochim.*  
1019 *Acta*, 150, 171–191, 2015.
- 1020 Urey, H.C., Lowenstam, H.A., Epstein, S. & McKinney, C.R.: Measurement of paleo-temperature and  
1021 temperatures of the upper cretaceous of England, Denmark, and the southeastern United-States. *Geol. Soc.*  
1022 *Am. Bull.*, 62, 399-416, 1951.
- 1023 Wang, B.-S., You, C.-F., Huang, K.-F., Wu, S.-F., Aggarwal, S. K., Chung, C.-H. and Lin, P.-Y., Direct  
1024 separation of boron from Na- and Ca-rich matrices by sublimation for stable isotope measurement by MC-  
1025 ICP-MS, *Talanta*, 82, 1378–1384, 2010.
- 1026 Wang, G., Cao, W., Yang, D. and Xu, D., Variation in downwelling diffuse attenuation coefficient in the  
1027 northern South China Sea, *Chinese J. Oceanol. Limnol.*, 26, 323–333, 2008.
- 1028 Weare, B. C., Strub, P. T. and Samuel, M. D., Annual Mean Surface Heat Fluxes in the Tropical Pacific Ocean,  
1029 *J. Phys. Oceanogr.*, 11, 705–717, 1981.
- 1030 Wei, G., McCulloch, M. T., Mortimer, G., Deng, W. and Xie, L., Evidence for ocean acidification in the Great  
1031 Barrier Reef of Australia, *Geochim. Cosmochim. Acta*, 73, 2332–2346, 2009.
- 1032 Wilson, D. J., Piotrowski, A. M., Galy, A. and McCave, I. N., A boundary exchange influence on deglacial  
1033 neodymium isotope records from the deep western Indian Ocean, *Earth Planet. Sci. Lett.*, 341–344, 35–47,  
1034 2012.
- 1035 Wolf-Gladrow, D. A., Riebesell, U., Burkhardt, S. and Buma, J., Direct effects of CO<sub>2</sub> concentration on growth  
1036 and isotopic composition of marine plankton, *Tellus B Chem. Phys. Meteorol.*, 51, 461–476, 1999.
- 1037 Yu, J., Menviel, L., Jin, Z. D., Thornalley, D. J. R., Barker, S., Marino, G., Rohling, E. J., Cai, Y., Zhang, F.,  
1038 Wang, X., Dai, Y., Chen, P. and Broecker, W. S., Sequestration of carbon in the deep Atlantic during the  
1039 last glaciation, *Nat. Geosci.*, 9, 319–324, 2016.

- 1040 Yu, J., Thornalley, D. J. R., Rae, J. W. B. and McCave, N. I., Calibration and application of B/Ca, Cd/Ca, and  $\delta$   
1041  $^{11}\text{B}$  in *Neogloboquadrina pachyderma* (sinistral) to constrain  $\text{CO}_2$  uptake in the subpolar North Atlantic  
1042 during the last deglaciation, *Paleoceanography*, 28, 237–252, 2013.
- 1043 Yu, J., Foster, G. L., Elderfield, H., Broecker, W. S. and Clark, E., An evaluation of benthic foraminiferal B/Ca  
1044 and  $\delta^{11}\text{B}$  for deep ocean carbonate ion and pH reconstructions, *Earth Planet. Sci. Lett.*, 293, 114–120, 20,  
1045 2010.
- 1046 Yu, J., Elderfield, H., Hönisch, B., B/Ca in planktonic foraminifera as a proxy for surface seawater pH.  
1047 *Paleoceanography* 22, PA2202, 2007.
- 1048 Yu, J., Day, J., Greaves, M. and Elderfield, H., Determination of multiple element/calcium ratios in foraminiferal  
1049 calcite by quadrupole ICP-MS, *Geochemistry, Geophys. Geosystems* 6, 2005.
- 1050 Zeebe, R. E. and Wolf-Gladrow, D., *CO<sub>2</sub> in Seawater: Equilibrium, Kinetics, Isotopes* Elsevier Oceanography  
1051 Series 65, Amsterdam, 2001.
- 1052 Zeebe, R. E., Wolf-Gladrow, D. A., Bijma, J. and Hönisch, B., Vital effects in foraminifera do not compromise  
1053 the use of  $\delta^{11}\text{B}$  as a paleo- pH indicator: Evidence from modeling, *Paleoceanography*, 18, 2003.

1054 **Figure caption**

1055  
1056 **Figure 1:** (A) Speciation of  $B(OH)_3$  and  $B(OH)_4^-$  as function of seawater pH (total scale), (B)  $\delta^{11}B$  of dissolved  
1057 inorganic boron species as a function of seawater pH, (C) sensitivity of  $\delta^{11}B$  of  $B(OH)_4^-$  for a pH ranging from 7.6  
1058 to 8.4.  $T=25^\circ C$ ,  $S=35$ ,  $\delta^{11}B=39.61 \text{ ‰}$  (Foster et al., 2010), dissociation constant  $\alpha = 1.0272$  (Klochko et al., 2006).

1059  
1060 **Figure 2:** Map showing locations of the core-tops used in this study (white diamonds). Red open circles represent  
1061 the sites used for *in situ* carbonate parameters from GLODAP database (Key et al., 2004).

1062  
1063 **Figure 3:** Pre-industrial data versus depth for the sites used in this study. The figure shows seasonal temperatures  
1064 (extracted from World Ocean Database 2013), density anomaly ( $kg/m^3$ ), pre-industrial pH and pre-industrial  $\delta^{11}B$   
1065 of  $H_4BO_4^-$  (calculated from the GLODAP database and corrected for anthropogenic inputs). Dotted lines are the  
1066 calculated uncertainties based on errors on TA and DIC from the GLODAP database.

1067  
1068 **Figure 4:** Boron isotopic measurements of mixed-layer foraminifera plotted against  $\delta^{11}B_{borate}$ .  $\delta^{11}B_{borate}$  was  
1069 characterized by determination of the calcification depth of foraminifera utilizing data presented in Fig. 3. A) *G.*  
1070 *ruber*, B) *T. sacculifer*, C) *O. universa*. Mono-specific calibrations (Table 3) and error bars on  $\delta^{11}B_{borate}$  were  
1071 derived utilizing the wild bootstrap code from Henehan et al. (2016), while errors on the  $\delta^{11}B_{carbonate}$  for this study  
1072 are reported as  $2\sigma$  of measured AE121 standards during the session of the sample. Calibrations were also derived  
1073 on the 250-400 size fraction for *G. ruber* and *T. sacculifer* (black dashed lines). Data reported on those graphs  
1074 have been measured with an MC-ICP-MS.

1075  
1076 **Figure 5:** Boron isotopic measurements of deep-dwelling foraminifera ( $\delta^{11}B_{carbonate}$ ) plotted against  $\delta^{11}B_{borate}$ .  
1077  $\delta^{11}B_{borate}$  was constrained using foraminiferal calcification depths. A) *P. obliquiloculata*, B) *G. menardii*, C) *N.*  
1078 *dutertrei*, D) *G. tumida* and E) Compilation of deep dweller species. Mono-specific calibrations are summarized  
1079 in Table 3.

1080  
1081 **Figure 6:** Boxplots of B/Ca ratios for multiple foraminifera species., including *T. sacculifer* (this study; Foster et  
1082 al., 2008; Ni et al; 2007; Seki et al., 2010), *G. ruber* (this study; Babila et al., 2014; Foster et al., 2008; Ni et al.,  
1083 2007), *G. inflata*, *G. bulloides* (Yu et al., 2007), *N. pachyderma* (Hendry et al., 2009; Yu et al., 2013), *N. dutertrei*  
1084 (this study; Foster et al., 2008), *O. universa*, *P.obliquiloculata*, *G. menardii*, *G. tumida* (this study).

1085  
1086 **Figure 7:** A) Boxplot showing the calculated microenvironment pH difference ( $\Delta$ microenvironment pH) between  
1087 microenvironment and external pH based on the  $\delta^{11}B$  data. B) This figure shows that a decrease in insolation can  
1088 explain the low  $\delta^{11}B$  from the WEP. Light penetration profile in the Western Pacific, with  $E_0$  in the WEP of  $220$   
1089  $J.s^{-1}.m^{-2}$  (Weare et al., 1981) and a light attenuation coefficient of  $0.028 (m^{-1})$  (Wang et al., 2008). Theoretical  
1090 depths were calculated for a decrease in microenvironment pH of  $\Delta pH_1 = -0.02$  (e.g. WP07-a);  $\Delta pH_1 = -0.04$  (e.g.  
1091 A14),  $\Delta pH_2 = -0.06$  (e.g. 806A). Light penetration corresponding to  $E_c$  is  $\sim 12\%$ ,  $\Delta pH_0 \sim 7\%$ ,  $\Delta pH_1 \sim 5\%$ ,  $\Delta pH_2 \sim 1\%$   
1092 respective calcification depth are 75m, 90m, 110m and 150m. Grey band is the calcification depth calculated that

1093 explains the  $\Delta$  microenvironment pH from  $\Delta\text{pH}_0$  to  $\Delta\text{pH}_2$ . Dotted lines show the range of the calcification depth  
1094 for *T. sacculifer* (w/o sacc) in the WEP utilized in this study.

1095

1096 **Figure 8:** Water depth pH profiles reconstructed at every site applying the mono-specific calibrations derived from  
1097 our results (Table 3). Figure is showing measured  $\delta^{11}\text{B}_{\text{calcite}}$ ,  $\delta^{11}\text{B}_{\text{borate}}$  calculated according to different calibrations  
1098 (see Table 3 and text), calculated pH based on  $\delta^{11}\text{B}$  ( $\text{pH}_{\delta^{11}\text{B}}$ ) and  $\text{pCO}_2$  calculated from  $\text{pH}_{\delta^{11}\text{B}}$  and alkalinity.

1099

1100 **Figure 9:** Evaluation of the reconstructed parameters,  $\delta^{11}\text{B}_{\text{borate}}$ , pH and  $\text{pCO}_2$  versus *in situ* parameter calculated  
1101 in Fig. 8 (based on  $\delta^{11}\text{B}$  and alkalinity). The recalculated parameters are consistent with *in situ* data, except for *G.*  
1102 *rubra*, and this variability might be explained by the different test sizes within measured size fractions.

1103 **Table caption**

1104

1105 **Table 1:** Box-core information

1106

1107 **Table 2:** Analytical results of  $\delta^{13}\text{C}$ ,  $\delta^{18}\text{O}$ ,  $\delta^{11}\text{B}$  and elemental ratios Li/Ca, B/Ca and Mg/Ca

1108

1109 **Table 3:** Species-specific  $\delta^{11}\text{B}_{\text{carbonate}}$  to  $\delta^{11}\text{B}_{\text{borate}}$  calibrations from literature and from our data

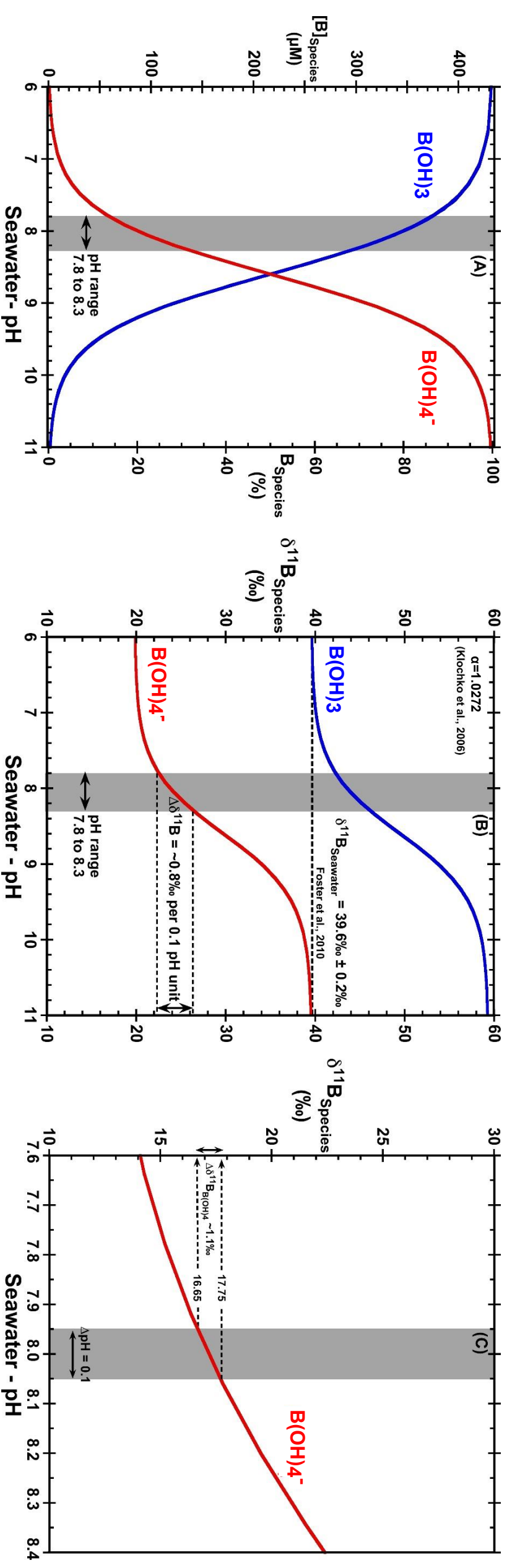


Figure 1



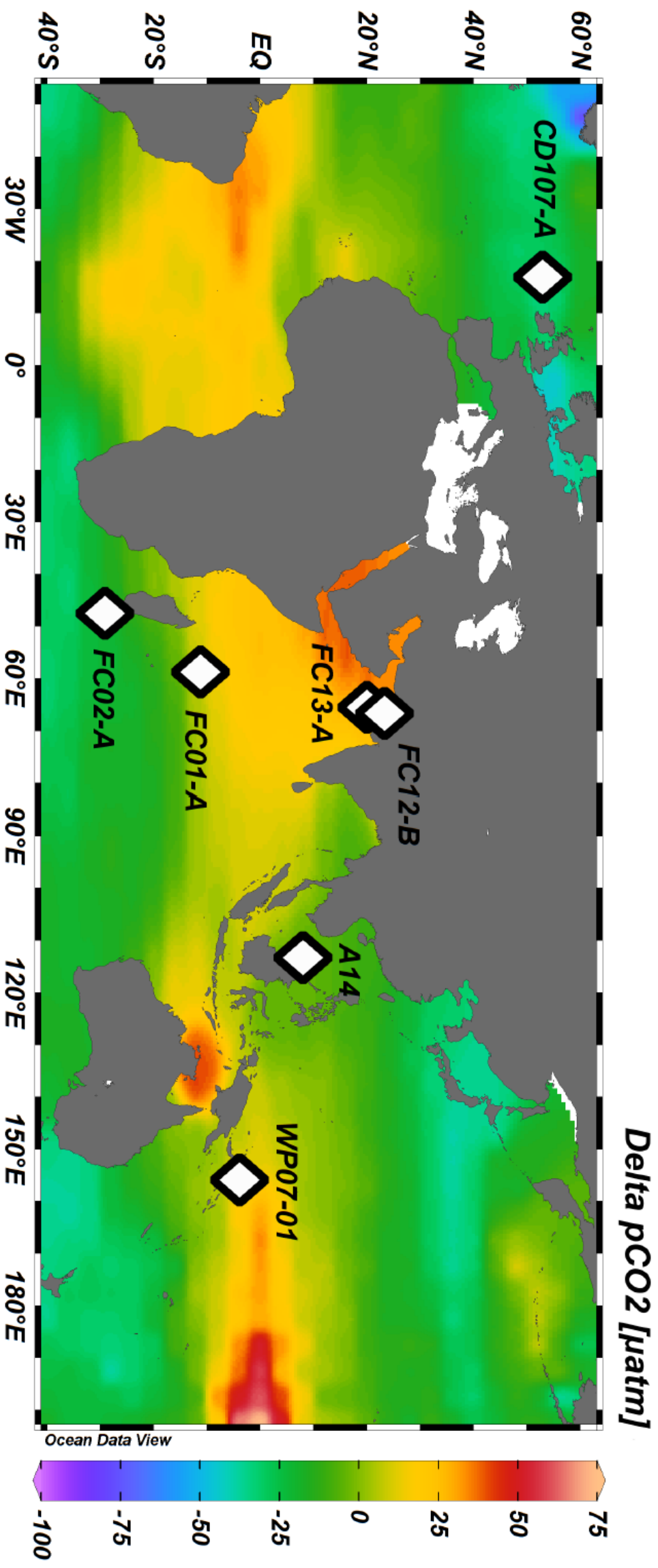


Figure 2

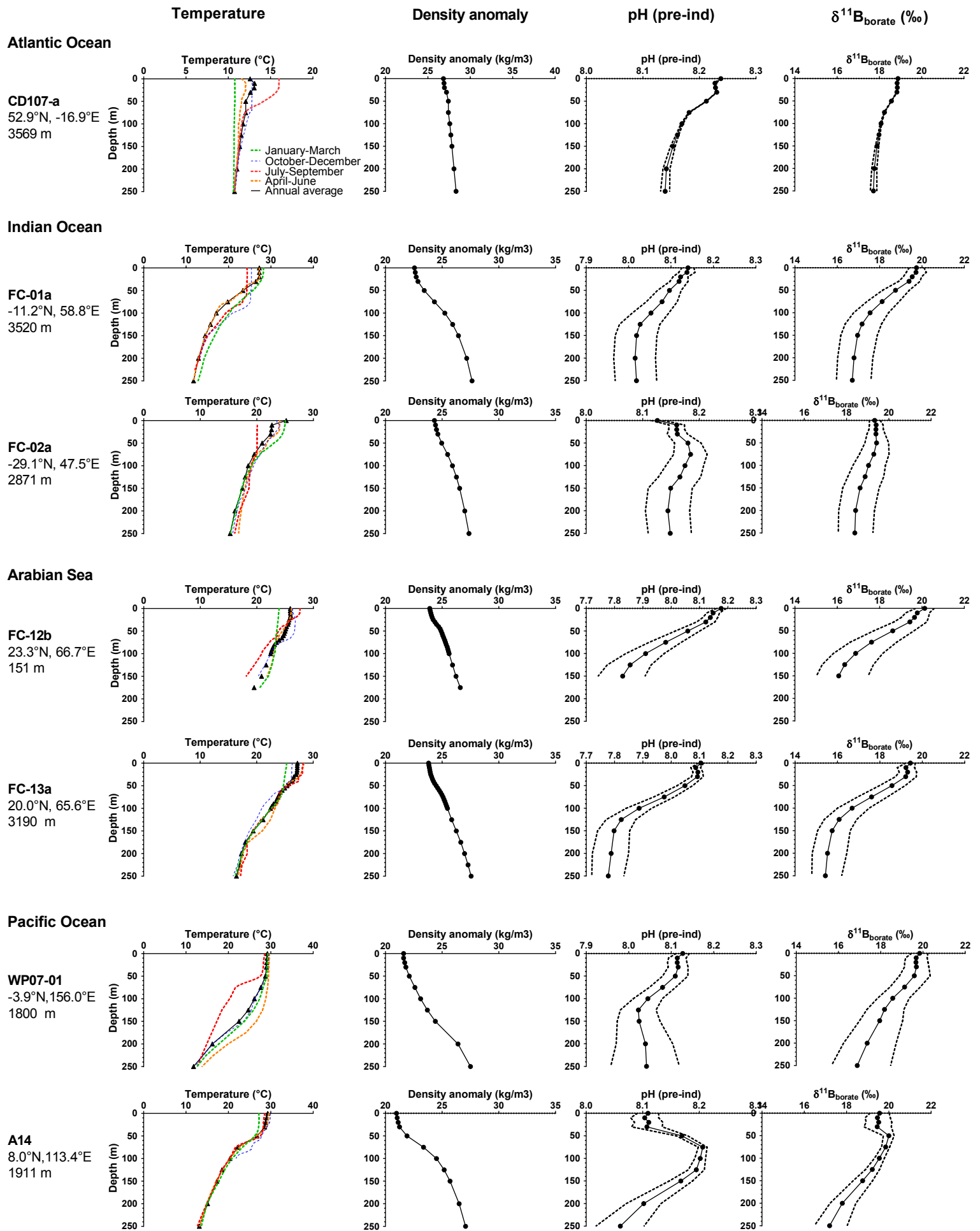
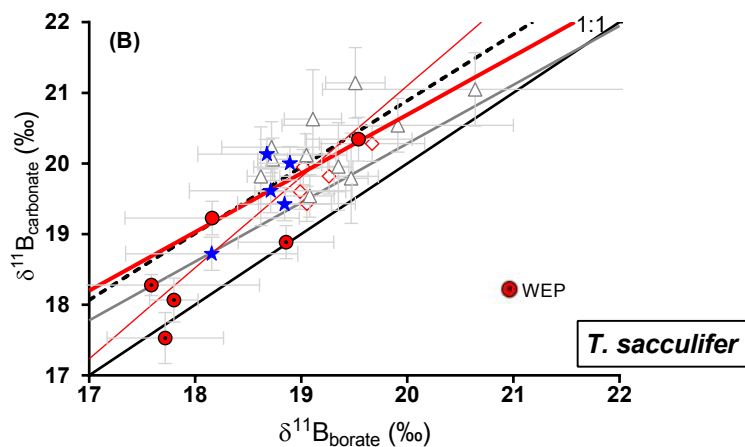
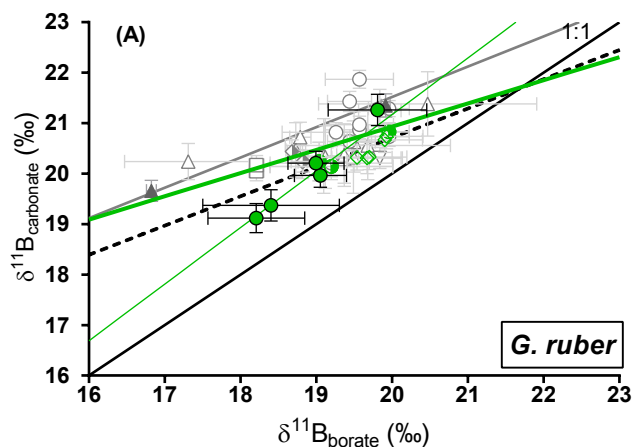
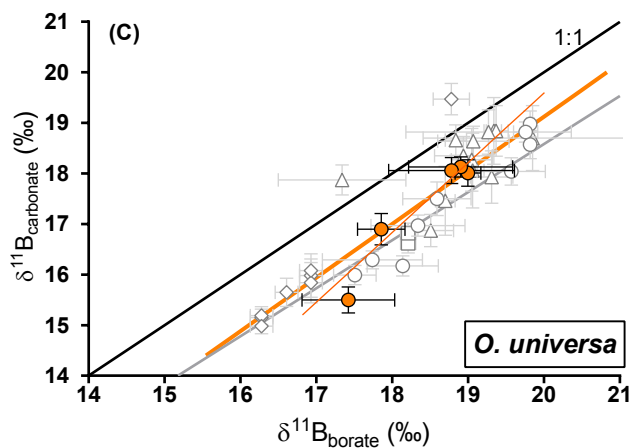


Figure 3 34



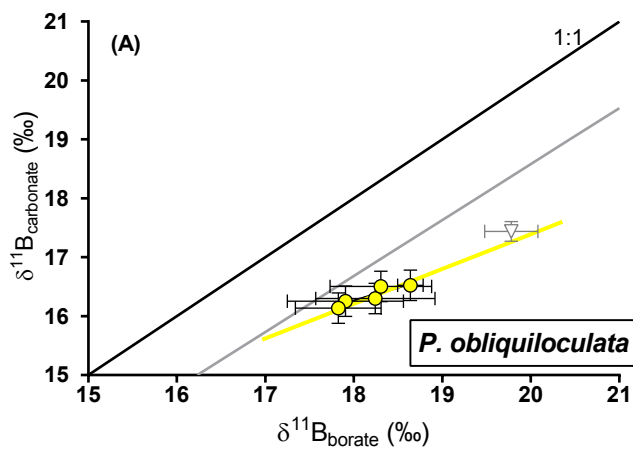
- $\delta^{11}\text{B}_{G. ruber}$  (core-top, 250-400 $\mu\text{m}$ , this study)
- ◇  $\delta^{11}\text{B}_{G. ruber}$  (core-top, 300-355 $\mu\text{m}$ , Foster et al., 2008)
- $\delta^{11}\text{B}_{G. ruber}$  (core-top, 250-300 $\mu\text{m}$ , Henehan et al., 2013)
- $\delta^{11}\text{B}_{G. ruber}$  (core-top, 250-455 $\mu\text{m}$ , Henehan et al., 2013)
- $\delta^{11}\text{B}_{G. ruber}$  (sediment trap, 250-355 $\mu\text{m}$ , Henehan et al., 2013)
- ◇  $\delta^{11}\text{B}_{G. ruber}$  (tow, Henehan et al., 2013)
- ▲  $\delta^{11}\text{B}_{G. ruber}$  (culture, Henehan et al., 2013)
- ▽  $\delta^{11}\text{B}_{G. ruber}$  (grab sample, 250-355 $\mu\text{m}$ , Henehan et al., 2013)
- △  $\delta^{11}\text{B}_{G. ruber}$  (core-top, 315-355 $\mu\text{m}$ , Raitsch et al., 2018)
- $G. ruber$  calibration line (all data, this study, 250-455)
- $G. ruber$  calibration line (core-top, this study, 250-400 $\mu\text{m}$ )
- $G. ruber$  calibration line (culture, Henehan et al., 2013)
- - -  $G. ruber$  calibration line (this study, 250-300 $\mu\text{m}$  from Henehan et al., 2013)

- $\delta^{11}\text{B}_{T. sacculifer}$  (w/o sacc) (core-top, 250-400 $\mu\text{m}$ , this study)
- △  $\delta^{11}\text{B}_{T. sacculifer}$  (w/o sacc) (core-top, 315-355 $\mu\text{m}$ , Raitsch et al., 2018)
- ★  $\delta^{11}\text{B}_{T. sacculifer}$  (sacc) (core-top, 250-400 $\mu\text{m}$ , this study)
- ◇  $\delta^{11}\text{B}_{T. sacculifer}$  (sacc) (core-top, 500-600 $\mu\text{m}$ , Foster et al., 2008)
- $T. sacculifer$  (w/o sacc and sacc) calibration line (all data, 250-600 $\mu\text{m}$ , this study)
- $T. sacculifer$  (w/o sacc and sacc) calibration line (core-top, 250-400 $\mu\text{m}$ , this study)
- $T. sacculifer$  (sacc) calibration line (Martinez-Boti et al., 2015)
- - -  $T. sacculifer$  (w/o sacc and sacc) calibration line 250-400  $\mu\text{m}$  (this study and Raitsch et al., 2018)

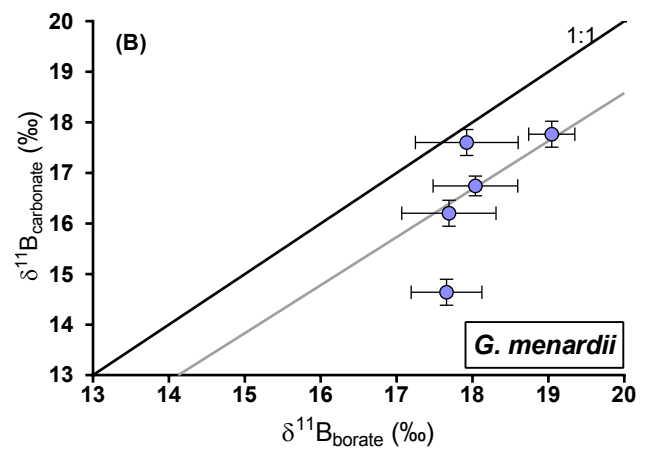


- $\delta^{11}\text{B}_{O. universa}$  (core-top, this study)
- $\delta^{11}\text{B}_{O. universa}$  (core-top, Henehan et al., 2016)
- $\delta^{11}\text{B}_{O. universa}$  (sediment trap, Henehan et al., 2016)
- ◇  $\delta^{11}\text{B}_{O. universa}$  (tow, Henehan et al., 2016)
- △  $\delta^{11}\text{B}_{O. universa}$  (core-top, Raitsch et al., 2018)
- $O. universa$  calibration line (core-top, this study)
- $O. universa$  calibration line (this study, Henehan et al., 2016, Raitsch et al., 2018)
- $O. universa$  calibration line (wild, Henehan et al., 2016)

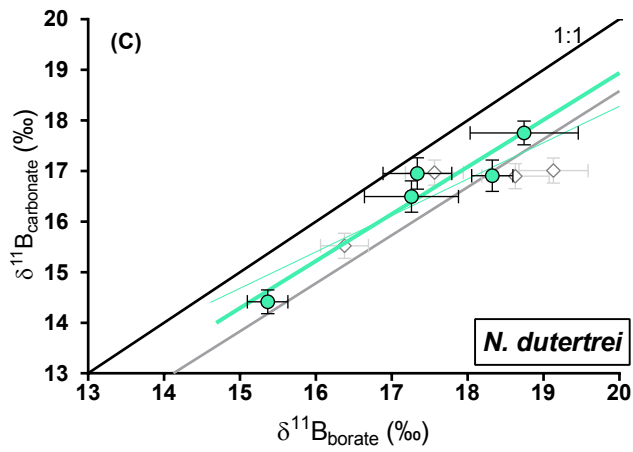
Figure 4



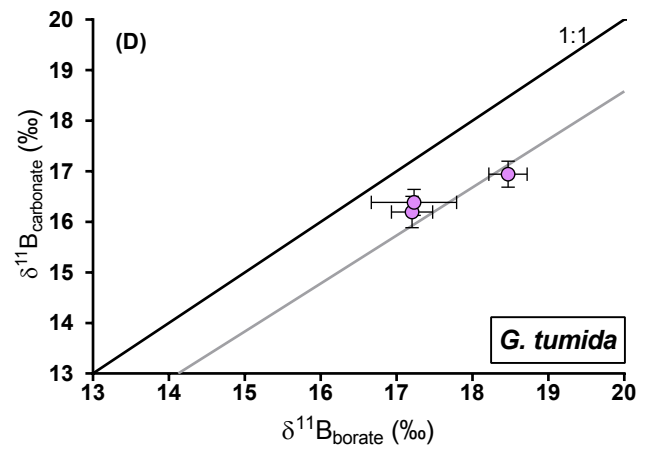
- $\delta^{11}\text{B}_{P.obliquiloculata}$  (Core-top, this study)
- ▽  $\delta^{11}\text{B}_{P.obliquiloculata}$  (Henehan et al., 2016)
- $P.obliquiloculata$  calibration line (this study, Henehan et al., 2016)
- $O.universa$  calibration curve (Henehan et al., 2016)



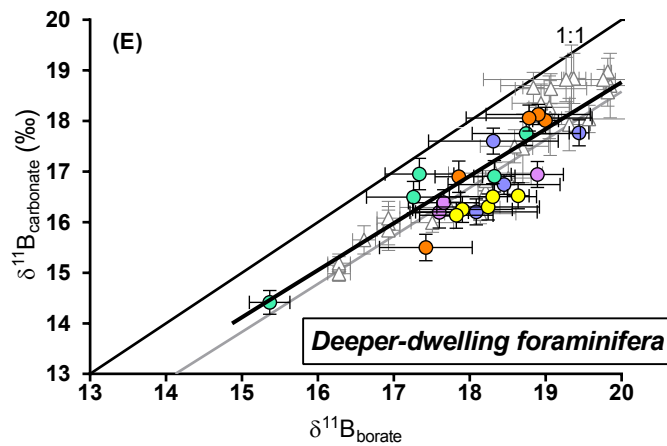
- $\delta^{11}\text{B}_{G.menardii}$  (this study)
- $O.universa$  calibration curve (Henehan et al., 2016)



- $\delta^{11}\text{B}_{N.dutertrei}$  (Core-top, this study)
- ◇  $\delta^{11}\text{B}_{N.dutertrei}$  (Core-top, Foster et al., 2008)
- $O.universa$  calibration line (This study)
- $O.universa$  calibration line (This study, Foster et al., 2008)
- $O.universa$  calibration line (Henehan et al., 2016)



- $\delta^{11}\text{B}_{G.tumida}$  (this study)
- $O.universa$  calibration curve (Henehan et al., 2016)



- $\delta^{11}\text{B}_{O.universa}$
- $\delta^{11}\text{B}_{P.obliquiloculata}$
- $\delta^{11}\text{B}_{N.dutertrei}$
- $\delta^{11}\text{B}_{G.menardii}$
- $\delta^{11}\text{B}_{G.tumida}$
- △  $\delta^{11}\text{B}_{\text{deep-dweller}}$  from literature
- Deep-dweller calibration line
- $O.universa$  calibration line (Henehan et al., 2016)

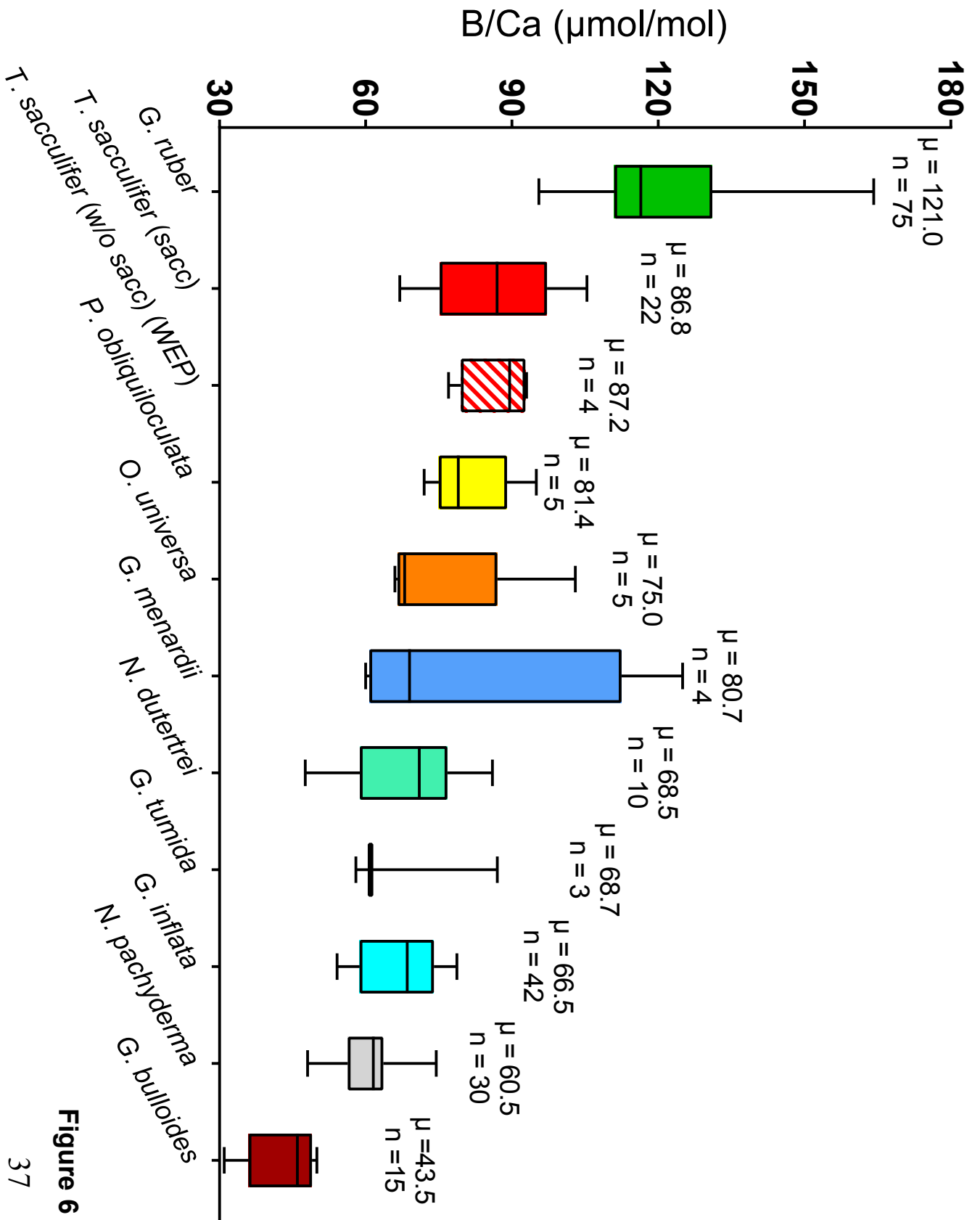


**Figure 6**

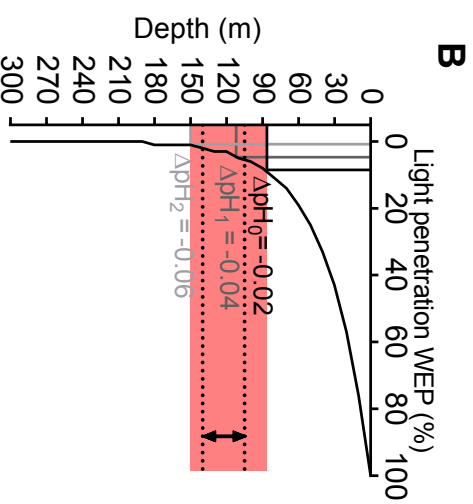
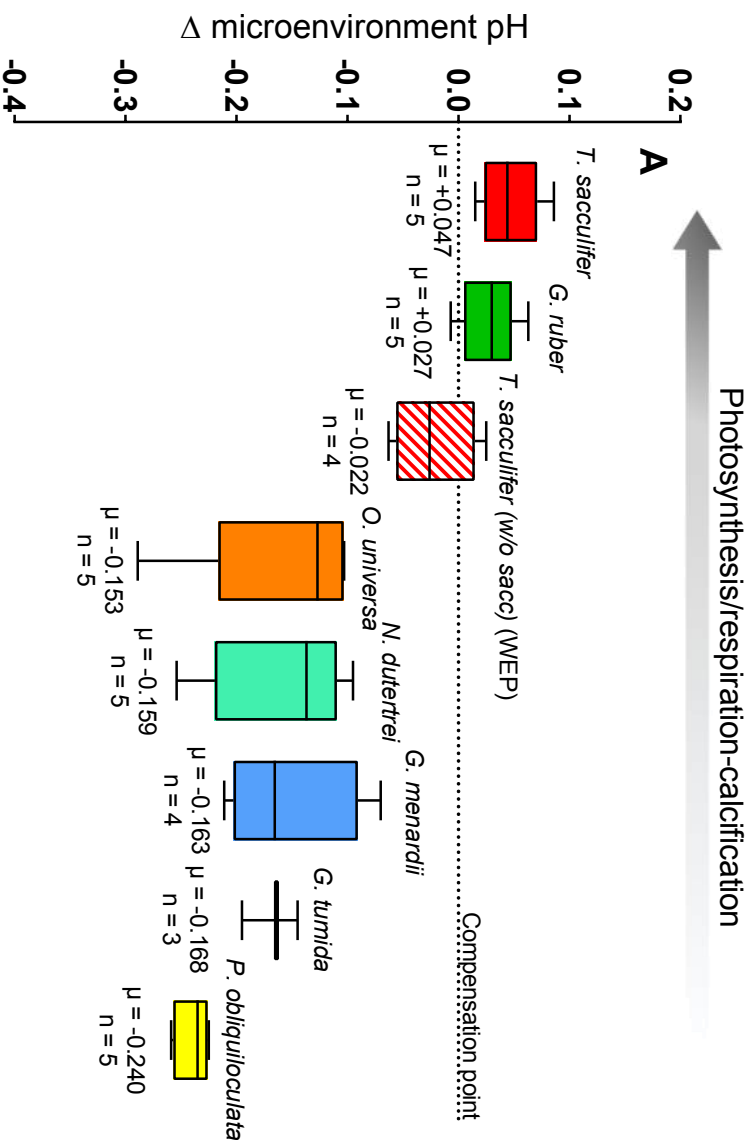


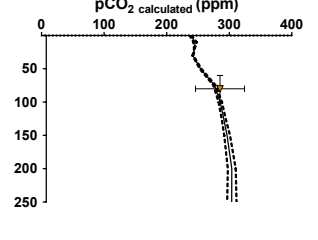
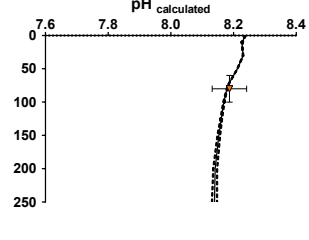
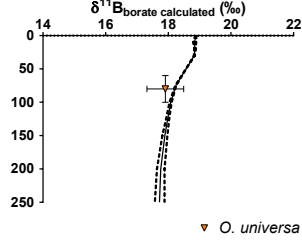
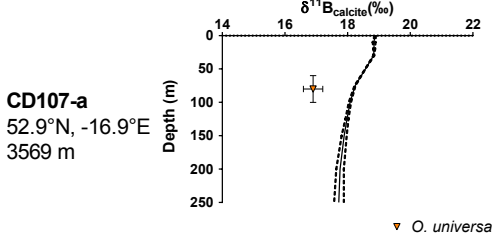
**Figure 7**

$\delta^{11}\text{B}_{\text{carbonate}}$  $\delta^{11}\text{B}_{\text{borate}}$ 

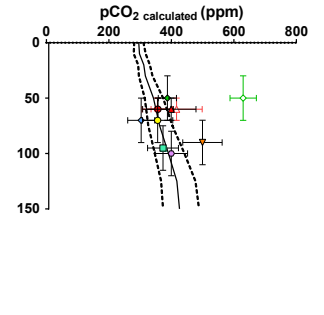
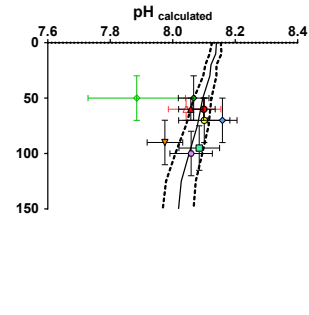
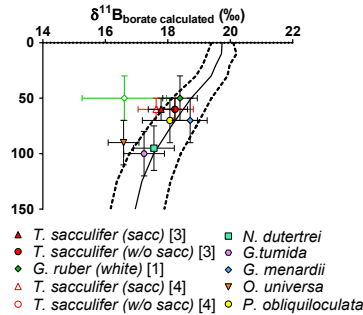
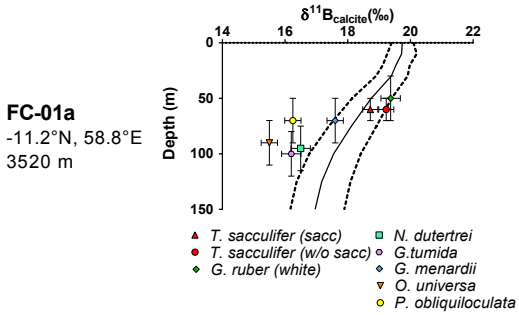
pH

 $\text{pCO}_2$ 

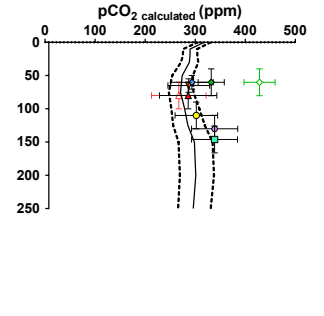
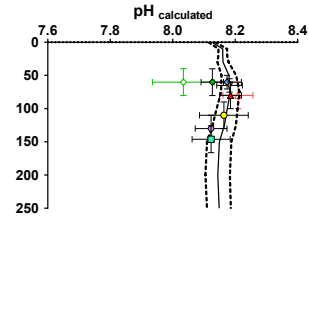
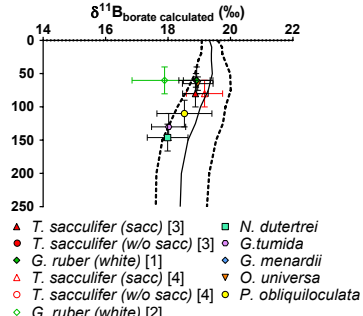
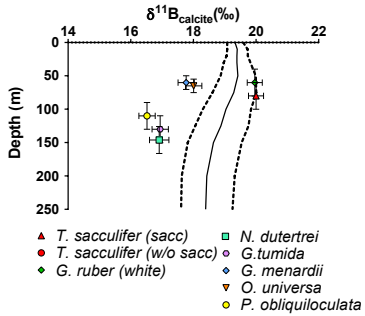
## Atlantic Ocean



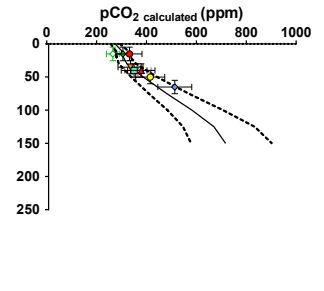
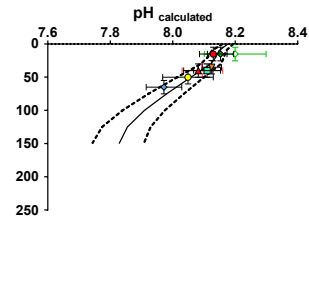
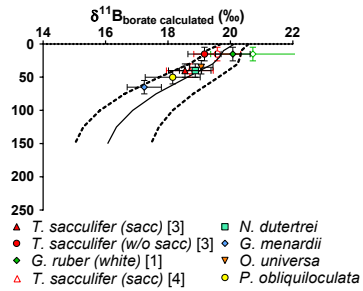
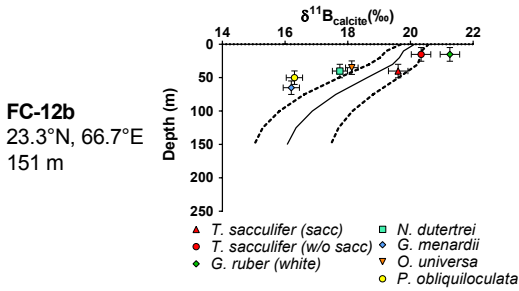
## Indian Ocean



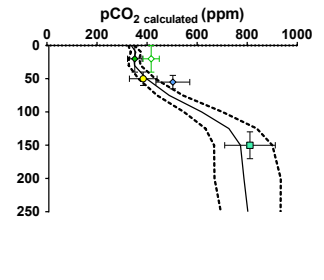
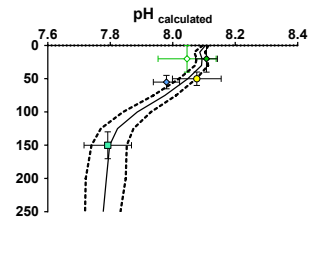
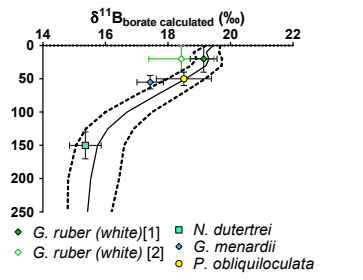
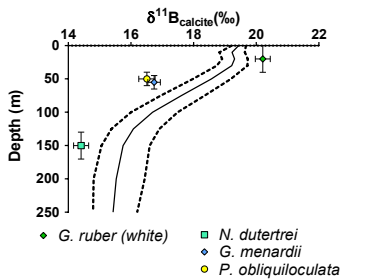
**FC-02a**  
-29.1°N, 47.5°E  
2871 m



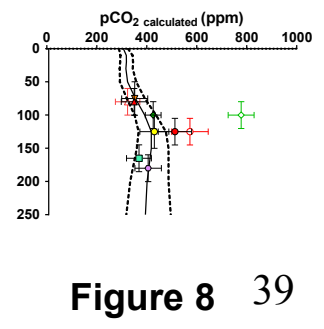
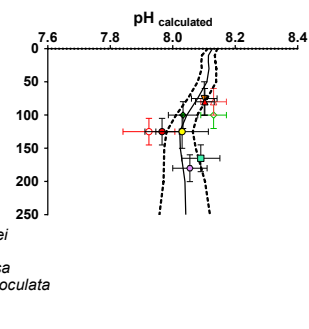
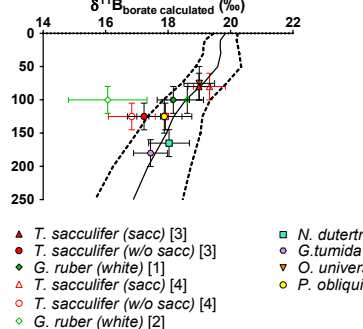
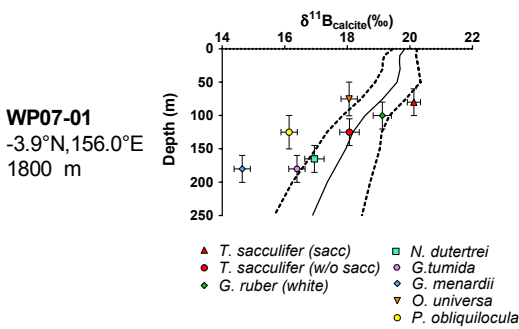
## Arabian Sea



**FC-13a**  
20.0°N, 65.6°E  
3190 m



## Pacific Ocean



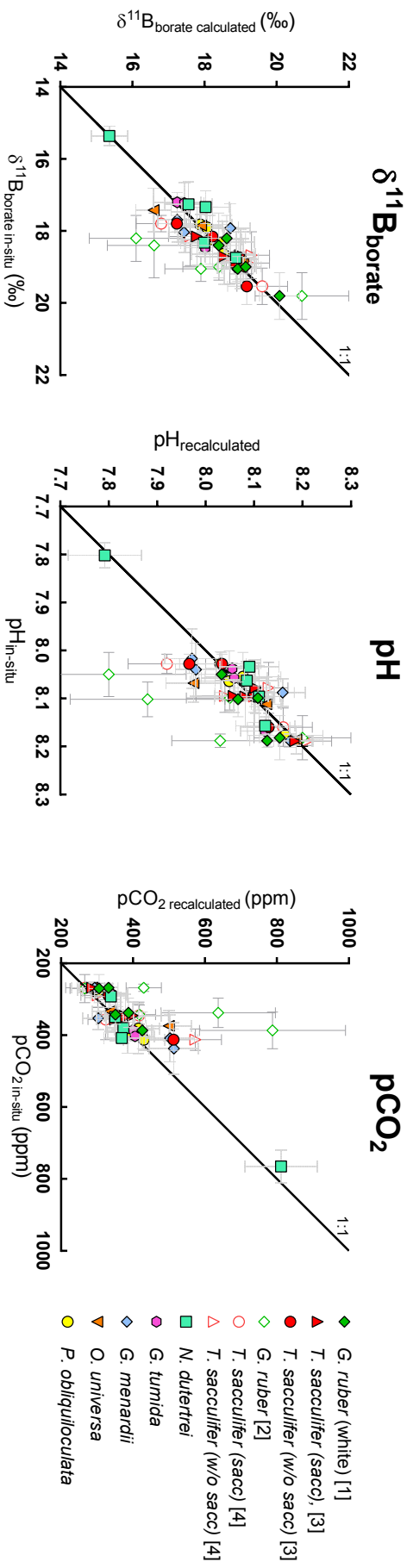


**Figure 9** 40



**Table 1**

<b>Label</b>	<b>Box-Core</b>	<b>Site</b>	<b>Latitude (N)</b>	<b>Longitude (E)</b>	<b>Depth (mbsl)</b>	<b>Oceanic Regime</b>	<b><sup>14</sup>C age (year)</b>
<i>Atlantic Ocean</i>							
CDI07-a	CDI07	A	52.92	-16.92	3569	non-upwelling	<3000 <sup>a</sup>
<i>Indian Ocean</i>							
FC-01a	WIND-33B	I	-11.21	58.77	3520	non-upwelling	
FC-02a	WIND-10B	K	-29.12	47.55	2871	non-upwelling	7252 ± 27 <sup>b</sup>
<i>Arabian Sea</i>							
FC-12b	CDI45	A150	23.30	66.70	151	seasonal upwelling	
FC-13a	CDI45	A3200	20.00	65.58	3190	seasonal upwelling	
<i>Pacific Ocean</i>							
WP07-01			-3.93	156.00	1800	non-upwelling	7300-8600 <sup>c</sup>
A14			8.02	113.39	1911	non-upwelling	7300-8600 <sup>c</sup>
806		A	0.32	159.36	2521	equatorial divergence	7300-8600 <sup>c</sup>
807		A	3.61	156.62	2804	equatorial divergence	7300-8600 <sup>c</sup>

<sup>a</sup>Thomson et al., 2000

<sup>b</sup>Wilson et al., 2012

<sup>c</sup>Age for core-top of site 806B from Lea et al., 2000

Table 2

Core	Species	Fraction size (µm)	$\delta^{13}\text{C}^{\text{ss}}$ (‰)	$\delta^{18}\text{O}^{\text{ss}}$ (‰)	$\delta^{11}\text{Bc}$ (‰)	$\delta^{11}\text{Bc}$ (‰)	$\delta^{11}\text{B}_{\text{average}}^{\text{ss}}$ (‰)	$\text{Li/Ca}^{\text{ss}}$ (µmol/mol)	$\text{B/Ca}^{\text{ss}}$ (µmol/mol)	$\text{Mg/Ca}^{\text{ss}}$ (µmol/mol)	
<b>Atlantic Ocean</b>											
CD107a	<i>O. universa</i>	>500	1.99 ± 0.03	1.25 ± 0.11	16.85 ± 0.31 (2SD, n=AE121=11)	16.95 ± 0.31 (2SD, n=AE121=11)	16.90 ± 0.22	13.9 ± 0.4	68 ± 7	3.60 ± 0.01	
<b>Indian Ocean</b>											
FC-01a	<i>G. ruber</i> (white ss)	250-300	1.37 ± 0.03	-1.32 ± 0.11	19.33 ± 0.31 (2SD, n=AE121=11)	19.41 ± 0.31 (2SD, n=AE121=11)	19.37 ± 0.22	15.4 ± 0.4	109 ± 7	3.98 ± 0.01	
FC-01a	<i>T. sacculifer</i> (sacc)	300-400	1.88 ± 0.03	-2.20 ± 0.11	18.71 ± 0.24 (2SD, n=AE121=10)	18.73 ± 0.24 (2SD, n=AE121=10)	18.72 ± 0.17	12.1 ± 0.4	87 ± 7	3.45 ± 0.01	
FC-01a	<i>T. sacculifer</i> (w/o sacc)	300-400	2.02 ± 0.03	-1.05 ± 0.11	19.13 ± 0.24 (2SD, n=AE121=10)	19.32 ± 0.24 (2SD, n=AE121=10)	19.23 ± 0.17	12.1 ± 0.4	82 ± 7	3.42 ± 0.01	
FC-01a	<i>O. universa</i>	>500			15.50 ± 0.26 (2SD, n=AE121=14)		15.50 ± 0.26				
FC-01a	<i>P. obliquiloculata</i>	300-400	1.00 ± 0.03	-0.55 ± 0.11	16.40 ± 0.26 (2SD, n=AE121=14)	16.10 ± 0.26 (2SD, n=AE121=14)	16.25 ± 0.18	15.4 ± 0.4	78 ± 7	2.06 ± 0.01	
FC-01a	<i>G. menardi</i>	300-400	1.64 ± 0.03	0.43 ± 0.11	17.52 ± 0.26 (2SD, n=AE121=14)	17.69 ± 0.26 (2SD, n=AE121=14)	17.60 ± 0.18	12.7 ± 0.4	63 ± 7	2.26 ± 0.01	
FC-01a	<i>N. duterrei</i>	300-400	1.28 ± 0.03	-0.43 ± 0.11	16.40 ± 0.31 (2SD, n=AE121=11)	16.59 ± 0.31 (2SD, n=AE121=11)	16.50 ± 0.22	18.6 ± 0.4	73 ± 7	1.81 ± 0.01	
FC-01a	<i>G. tumida</i>	300-400	1.29 ± 0.03	-0.53 ± 0.11	16.21 ± 0.31 (2SD, n=AE121=11)	16.18 ± 0.31 (2SD, n=AE121=11)	16.20 ± 0.22	10.0 ± 0.4	61 ± 7	1.79 ± 0.01	
FC-02a	<i>G. ruber</i> (white ss)	250-300	0.30 ± 0.03	-1.40 ± 0.11	20.02 ± 0.24 (2SD, n=AE121=10)	19.90 ± 0.24 (2SD, n=AE121=10)	19.96 ± 0.17	18.2 ± 0.4	125 ± 7	3.47 ± 0.01	
FC-02a	<i>T. sacculifer</i> (sacc)	300-400	1.43 ± 0.03	-1.60 ± 0.11	20.07 ± 0.24 (2SD, n=AE121=10)	19.93 ± 0.24 (2SD, n=AE121=10)	20.00 ± 0.17	14.2 ± 0.4	106 ± 7	3.30 ± 0.01	
FC-02a	<i>T. sacculifer</i> (w/o sacc)	300-400	1.52 ± 0.03	-1.40 ± 0.11	23.23 ± 0.24 (2SD, n=AE121=10)	23.22 ± 0.24 (2SD, n=AE121=10)	23.22 ± 0.17	13.7 ± 0.4	106 ± 7	3.34 ± 0.01	
FC-02a	<i>O. universa</i>	>500	1.79 ± 0.03	0.02 ± 0.11	18.05 ± 0.26 (2SD, n=AE121=14)	17.97 ± 0.26 (2SD, n=AE121=14)	18.01 ± 0.18	14.8 ± 0.4	67 ± 7	4.40 ± 0.01	
FC-02a	<i>P. obliquiloculata</i>	300-400	0.34 ± 0.03	0.56 ± 0.11	16.35 ± 0.26 (2SD, n=AE121=14)	16.69 ± 0.26 (2SD, n=AE121=14)	16.52 ± 0.18	16.6 ± 0.4	83 ± 7	2.33 ± 0.01	
FC-02a	<i>G. menardi</i>	300-400	1.73 ± 0.03	-0.51 ± 0.11	17.77 ± 0.26 (2SD, n=AE121=14)	17.77 ± 0.26 (2SD, n=AE121=14)	17.77 ± 0.26	15.8 ± 0.4	125 ± 7	2.21 ± 0.01	
FC-02a	<i>N. duterrei</i>	300-400	1.03 ± 0.03	-0.55 ± 0.11	16.78 ± 0.31 (2SD, n=AE121=11)	17.03 ± 0.31 (2SD, n=AE121=11)	16.91 ± 0.22	18.6 ± 0.4	82 ± 7	2.13 ± 0.01	
FC-02a	<i>G. tumida</i>	300-400	1.64 ± 0.03	-0.28 ± 0.11	16.93 ± 0.26 (2SD, n=AE121=14)	16.95 ± 0.26 (2SD, n=AE121=14)	16.94 ± 0.18	15.6 ± 0.4	87 ± 7	1.90 ± 0.01	
<b>Arabian Sea</b>											
FC-12b	<i>G. ruber</i> (white ss)	250-300	0.58 ± 0.03	-2.82 ± 0.11	21.30 ± 0.31 (2SD, n=AE121=11)	21.23 ± 0.31 (2SD, n=AE121=11)	21.26 ± 0.22	19.5 ± 0.4	164 ± 7	5.76 ± 0.01	
FC-12b	<i>G. sacculifer</i> (s)	300-400	1.76 ± 0.03	-2.15 ± 0.11	19.65 ± 0.31 (2SD, n=AE121=11)	19.57 ± 0.31 (2SD, n=AE121=11)	19.61 ± 0.22	14.6 ± 0.4	101 ± 7	4.28 ± 0.01	
FC-12b	<i>T. sacculifer</i> (w/o sacc)	300-400	1.97 ± 0.03	-2.19 ± 0.11	20.32 ± 0.31 (2SD, n=AE121=11)	20.37 ± 0.31 (2SD, n=AE121=11)	20.34 ± 0.22	16.7 ± 0.4	116 ± 7	4.90 ± 0.01	
FC-12b	<i>O. universa</i>	>500	1.89 ± 0.03	-1.59 ± 0.11	18.13 ± 0.20 (2SD, n=AE121=6)	18.13 ± 0.20 (2SD, n=AE121=6)	18.13 ± 0.20	13.6 ± 0.4	103 ± 7	6.91 ± 0.01	
FC-12b	<i>P. obliquiloculata</i>	300-400	0.5 ± 0.03	-1.58 ± 0.11	16.45 ± 0.26 (2SD, n=AE121=14)	16.15 ± 0.26 (2SD, n=AE121=14)	16.30 ± 0.18	16.7 ± 0.4	95 ± 7	3.61 ± 0.01	
FC-12b	<i>G. menardi</i>	300-400	1.05 ± 0.03	-0.97 ± 0.11	16.2 ± 0.26 (2SD, n=AE121=14)	16.2 ± 0.26 (2SD, n=AE121=14)	16.20 ± 0.26	14.8 ± 0.4	75 ± 7	3.44 ± 0.01	
FC-12b	<i>N. duterrei</i>	300-400	1.35 ± 0.03	-1.57 ± 0.11	17.77 ± 0.24 (2SD, n=AE121=10)	17.73 ± 0.24 (2SD, n=AE121=10)	17.75 ± 0.17	17.1 ± 0.4	75 ± 7	3.25 ± 0.01	
FC-13a	<i>G. ruber</i> (white ss)	250-300	0.08 ± 0.03	-3.71 ± 0.11	20.27 ± 0.24 (2SD, n=AE121=10)	20.15 ± 0.24 (2SD, n=AE121=10)	20.21 ± 0.17	16.4 ± 0.4	147 ± 7	4.52 ± 0.01	
FC-13a	<i>T. sacculifer</i> (w/o sacc)	300-400	1.59 ± 0.03	-2.46 ± 0.11	17.85 ± 0.29 (2SD, n=AE121=12)	17.85 ± 0.29 (2SD, n=AE121=12)	17.85 ± 0.29	15.7 ± 0.4	121 ± 7	5.49 ± 0.01	
FC-13a	<i>P. obliquiloculata</i>	300-400	0.00 ± 0.03	-0.97 ± 0.11	16.51 ± 0.26 (2SD, n=AE121=14)	16.50 ± 0.26 (2SD, n=AE121=14)	16.51 ± 0.18	18.7 ± 0.4	79 ± 7	4.43 ± 0.01	
FC-13a	<i>G. menardi</i>	300-400	0.75 ± 0.03	-1.07 ± 0.11	16.74 ± 0.20 (2SD, n=AE121=6)	16.74 ± 0.20 (2SD, n=AE121=6)	16.74 ± 0.20	9.2 ± 0.4	60 ± 7	1.99 ± 0.01	
FC-13a	<i>N. duterrei</i>	300-400	0.71 ± 0.03	-1.41 ± 0.11	14.43 ± 0.24 (2SD, n=AE121=10)	14.40 ± 0.24 (2SD, n=AE121=10)	14.41 ± 0.17	15.7 ± 0.4	69 ± 7	1.98 ± 0.01	
<b>Pacific Ocean</b>											
WP07-a	<i>G. ruber</i> (white ss)	250-400			19.12 ± 0.29 (2SD, n=AE121=12)		19.12 ± 0.29	14.5 ± 0.4	144 ± 7	4.32 ± 0.01	
WP07-a	<i>T. sacculifer</i> (sacc)	250-400			20.13 ± 0.21 (2SD, n=AE121=11)		20.13 ± 0.21	12.7 ± 0.4	92 ± 7	4.44 ± 0.01	
WP07-a	<i>T. sacculifer</i> (w/o sacc)	250-400			18.10 ± 0.31 (2SD, n=AE121=11)		18.07 ± 0.22	12.3 ± 0.4	192 ± 7	4.51 ± 0.01	
WP07-a	<i>O. universa</i>	500-630			18.13 ± 0.26 (2SD, n=AE121=14)		17.99 ± 0.26 (2SD, n=AE121=14)	11.9 ± 0.4	71 ± 7	7.52 ± 0.01	
WP07-a	<i>P. obliquiloculata</i>	250-400			16.08 ± 0.26 (2SD, n=AE121=14)		16.19 ± 0.26 (2SD, n=AE121=14)	13.4 ± 0.4	72 ± 7	3.02 ± 0.01	
WP07-a	<i>G. menardi</i>	250-400			14.74 ± 0.26 (2SD, n=AE121=14)		14.53 ± 0.26 (2SD, n=AE121=14)	13.5 ± 0.4	85 ± 7	2.68 ± 0.01	
WP07-a	<i>N. duterrei</i>	250-400			16.91 ± 0.31 (2SD, n=AE121=11)		16.99 ± 0.31 (2SD, n=AE121=11)	21.7 ± 0.4	86 ± 7	3.66 ± 0.01	
WP07-a	<i>G. tumida</i>	250-400			16.45 ± 0.26 (2SD, n=AE121=14)		16.32 ± 0.26 (2SD, n=AE121=14)	10.6 ± 0.4	58 ± 7	2.55 ± 0.01	
806A	<i>T. sacculifer</i> (w/o sacc)	250-400			17.53 ± 0.36 (2SD, n=AE121=11)		17.53 ± 0.36	14.40 ± 0.4	77 ± 7	3.89 ± 0.01	
807A	<i>T. sacculifer</i> (w/o sacc)	250-400			18.38 ± 0.21 (2SD, n=AE121=11)		18.17 ± 0.21 (2SD, n=AE121=11)	18.28 ± 0.15	87 ± 7	4.24 ± 0.01	
A14	<i>G. ruber</i> (white ss)	250-400			18.91 ± 0.24 (2SD, n=AE121=10)		19.17 ± 0.24 (2SD, n=AE121=10)	19.04 ± 0.17	102 ± 7	3.91 ± 0.01	
A14	<i>T. sacculifer</i> (sacc)	250-400			19.53 ± 0.24 (2SD, n=AE121=10)		19.32 ± 0.24 (2SD, n=AE121=10)	19.42 ± 0.17	93 ± 7	3.76 ± 0.01	
A14	<i>T. sacculifer</i> (w/o sacc)	250-400			18.93 ± 0.24 (2SD, n=AE121=10)		18.84 ± 0.24 (2SD, n=AE121=10)	18.88 ± 0.17	12.3 ± 0.4	66 ± 7	6.59 ± 0.01
A14	<i>O. universa</i>	500-560			17.33 ± 0.26 (2SD, n=AE121=14)		17.08 ± 0.26 (2SD, n=AE121=14)	17.20 ± 0.18	11.3 ± 0.4	75 ± 7	1.99 ± 0.01
A14	<i>N. duterrei</i>	250-400			14.39 ± 0.31 (2SD, n=AE121=11)		14.39 ± 0.31	16.9 ± 0.4	75 ± 7	1.99 ± 0.01	

\* uncertainties given in 1SD (see text)

\*\* When two measurements were carried out uncertainty was calculated with  $A_{\text{a}} = \sqrt{(\sum (1/A_{\text{a}})^2)}$ , with only one measurement the error was determined on reproducibility of the AE121 standard

\*\*\*Uncertainty given in 2SD, calculated on the reproducibility of CamWuelessdorf (see text and table S3, ref in Misra et al., 2014)

Table 3

Species	Size Fraction ( $\mu\text{m}$ )	Material	Instrument (original)	Regression method	$\delta^{11}\text{B}_{\text{meas}} (\delta^{11}\text{B}_{\text{lake}})$	n	Calibration number	Reference
<i>G. ruber</i>	~380	Culture/core tops/plankton tows	MC-ICP-MS	Bootstrap	$\delta^{11}\text{B}_{\text{meas}} = \delta^{11}\text{B}_{\text{lake}} - 9.52 (\pm 2.02) / 0.6 (\pm 0.11)$	9	0	This study; Henahan et al., 2013
<i>G. ruber</i>	315-355	Core-tops	MC-ICP-MS	Bootstrap	$\delta^{11}\text{B}_{\text{meas}} = \delta^{11}\text{B}_{\text{lake}} - 11.78 (\pm 3.20) / 0.45 (\pm 0.16)$	5	1	Rätzsch et al., 2018
<i>T. sacculifer</i>	n.d.	Culture/artificial seawater enriched in B	N-TIMS	Bootstrap	$\delta^{11}\text{B}_{\text{meas}} = \delta^{11}\text{B}_{\text{lake}} - 3.94 (\pm 4.02) / 0.82 (\pm 0.22)$	40	2	Sanyal et al., 2001; refitted; Martinez-Boit et al., 2015
<i>T. sacculifer</i>	315-355	Core-tops	MC-ICP-MS	Bootstrap	$\delta^{11}\text{B}_{\text{meas}} = \delta^{11}\text{B}_{\text{lake}} - 8.86 (\pm 5.27) / 0.59 (\pm 0.21)$	11	3	Rätzsch et al., 2018
<i>O. universa</i>	no effect	Core-tops/plankton tows/sediment traps	MC-ICP-MS	Bootstrap	$\delta^{11}\text{B}_{\text{meas}} = \delta^{11}\text{B}_{\text{lake}} + 0.42 (\pm 2.85) / 0.95 (\pm 0.17)$	5	5	Henahan et al., 2016
<i>O. universa</i>	>425	Core-tops	MC-ICP-MS	Bootstrap	$\delta^{11}\text{B}_{\text{meas}} = \delta^{11}\text{B}_{\text{lake}} + 5.69 (\pm 7.51) / 1.26 (\pm 0.39)$	6	6	Rätzsch et al., 2018
<i>G. bulloides</i>	300-355	Core-top/sediment trap	MC-ICP-MS	Bootstrap	$\delta^{11}\text{B}_{\text{meas}} = \delta^{11}\text{B}_{\text{lake}} + 3.440 (\pm 4.584) / 1.074 (\pm 0.252)$	27	4	Martinez-Boit et al., 2015
<i>G. bulloides</i>	315-355	Core-tops	MC-ICP-MS	Bootstrap	$\delta^{11}\text{B}_{\text{meas}} = \delta^{11}\text{B}_{\text{lake}} + 3.81 (\pm 3.17) / 1.13 (\pm 0.72)$	9	7	Rätzsch et al., 2018
<i>N. pachyderma</i>	150-200	Core-tops	MC-ICP-MS	Bootstrap	$\delta^{11}\text{B}_{\text{meas}} = \delta^{11}\text{B}_{\text{lake}} + 3.38$	5	5	Yu et al., 2013
<i>G. ruber</i>	250-400	Core-tops	MC-ICP-MS	Bootstrap	$\delta^{11}\text{B}_{\text{meas}} = \delta^{11}\text{B}_{\text{lake}} - 9.11 (\pm 0.73) / 0.58 (\pm 0.91)$	9	0	This study; Henahan et al., 2013
<i>G. ruber</i>	250-400	Core-tops	MC-ICP-MS	Bootstrap	$\delta^{11}\text{B}_{\text{meas}} = \delta^{11}\text{B}_{\text{lake}} + 1.23 (\pm 0.59) / 1.12 (\pm 1.67)$	5	1	This study
<i>G. ruber</i>	250-455	Core-tops	MC-ICP-MS	Bootstrap	$\delta^{11}\text{B}_{\text{meas}} = \delta^{11}\text{B}_{\text{lake}} - 11.73 (\pm 0.83) / 0.46 (\pm 0.34)$	40	2	This study; Foster et al., 2008; Henahan et al., 2016; Rätzsch et al., 2018
<i>T. sacculifer (sacc and w/o sacc)</i>	250-400	Core-tops	MC-ICP-MS	Bootstrap	$\delta^{11}\text{B}_{\text{meas}} = \delta^{11}\text{B}_{\text{lake}} + 6.06 (\pm 0.25) / 1.38 (\pm 1.33)$	11	3	This study
<i>T. sacculifer (sacc and w/o sacc)</i>	250-400	Core-tops	MC-ICP-MS	Bootstrap	$\delta^{11}\text{B}_{\text{meas}} = \delta^{11}\text{B}_{\text{lake}} - 4.09 (\pm 0.86) / 0.83 (\pm 0.48)$	27	4	This study; Foster et al., 2008; Rätzsch et al., 2018
<i>N. aderneti</i>	300-400	Core-tops	MC-ICP-MS	Bootstrap	$\delta^{11}\text{B}_{\text{meas}} = \delta^{11}\text{B}_{\text{lake}} - 0.34 (\pm 1.83) / 0.93 (\pm 0.55)$	5	5	This study
<i>N. aderneti</i>	300-400	Core-tops	MC-ICP-MS	Bootstrap	$\delta^{11}\text{B}_{\text{meas}} = \delta^{11}\text{B}_{\text{lake}} - 3.88 (\pm 0.65) / 0.72 (\pm 0.74)$	9	6	This study; Foster et al., 2008
<i>O. universa</i>	400-600	Core-tops	MC-ICP-MS	Bootstrap	$\delta^{11}\text{B}_{\text{meas}} = \delta^{11}\text{B}_{\text{lake}} + 8.01 (\pm 2.23) / 1.38 (\pm 2.67)$	5	7	This study
<i>O. universa</i>	400-600	Core-tops	MC-ICP-MS	Bootstrap	$\delta^{11}\text{B}_{\text{meas}} = \delta^{11}\text{B}_{\text{lake}} + 2.08 (\pm 0.59) / 1.06 (\pm 0.13)$	36	8	This study; Henahan et al., 2016; Rätzsch et al., 2018
<i>G. menardi</i>	400-600	Core-tops	MC-ICP-MS	Bootstrap	$\delta^{11}\text{B}_{\text{meas}} = \delta^{11}\text{B}_{\text{lake}} - 5.36 (\pm 1.36) / 0.65 (\pm 0.76)$	5	9	This study
<i>G. tuniata</i>	400-600	Core-tops	MC-ICP-MS	Bootstrap	$\delta^{11}\text{B}_{\text{meas}} = \delta^{11}\text{B}_{\text{lake}} - 6.33 (\pm 2.52) / 0.57 (\pm 1.12)$	3	10	This study
<i>P. obliquiloculata</i>	300-400	Core-tops	MC-ICP-MS	Bootstrap	$\delta^{11}\text{B}_{\text{meas}} = \delta^{11}\text{B}_{\text{lake}} - 5.59 (\pm 4.16) / 0.59 (\pm 0.65)$	6	11	This study; Henahan et al., 2016
<i>Deep-dweller</i>	300-600	Core-tops	MC-ICP-MS	Bootstrap	$\delta^{11}\text{B}_{\text{meas}} = \delta^{11}\text{B}_{\text{lake}} - 1.99 (\pm 0.13) / 0.82 (\pm 0.27)$	22	12	This study
<i>Deep-dweller</i>	300-600	Core-tops	MC-ICP-MS	Bootstrap	$\delta^{11}\text{B}_{\text{meas}} = \delta^{11}\text{B}_{\text{lake}} - 0.18 (\pm 0.61) / 0.95 (\pm 0.13)$	54	13	This study; Foster et al., 2008; Henahan et al., 2016; Rätzsch et al., 2018